1

SIX1 cooperates with RUNX1 and SMAD4 in cell fate commitment of Müllerian duct epithelium.

Jumpei Terakawa[1#], Vanida A. Serna[1], Devi Nair[1], Shigeru Sato[2], Kiyoshi Kawakami[2], Sally Radovick[3], Pascal Maire[4] and Takeshi Kurita[1*]

[1]Department of Cancer Biology and Genetics, The Comprehensive Cancer Center, The Ohio State University, Columbus, Ohio, United States of America

[2]Division of Biology, Center for Molecular Medicine, Jichi Medical University, Shimotsuke, Tochigi, Japan

[3] Department of Pediatrics, Robert Wood Johnson Medical School, The Child Health Institute of NJ, New Brunswick, New Jersey, United States of America

[4] Institut Cochin. INSERM U1016. CNRS UMR 8104. Université Paris Descartes., Paris, France

[#]Current address: Division of Transgenic Animal Science, Advanced Science Research Center, Kanazawa University, Kanazawa, Japan

Short title: SIX1 controls epithelial cell fate commitment in the Müllerian duct.

* Corresponding author

E-mail: takeshi.kurita@osumc.edu

2

Abstract

During female mammal reproductive tract development, epithelial cells of the lower Müllerian duct are committed to become stratified squamous epithelium of vagina and ectocervix, when the expression of ΔNp63 transcription factor is induced by mesenchymal cells. The absence of ΔNp63 expression leads to adenosis, the putative precursor of vaginal adenocarcinoma. Our previous studies with genetically engineered mouse models have established that fibroblast growth factor (FGF)/mitogen-activated protein kinase (MAPK), bone morphogenetic protein (BMP)/SMAD, and activin A/runt related transcription factor 1 (RUNX1) signaling pathways are independently required for ΔNp63 expression in Müllerian duct epithelium (MDE). Here we report that sine oculis homeobox homolog 1 (SIX1) plays a critical role in the activation of ΔNp63 locus in MDE as a downstream transcription factor of mesenchymal signals. In mouse developing reproductive tract, SIX1 expression was restricted to MDE of the future cervix and vagina. SIX1 expression was totally absent in SMAD4 null MDE and was reduced in RUNX1 null and FGFR2 null MDE, indicating that SIX1 is under the control of vaginal mesenchymal factors, BMP4, activin A and FGF7/10. Furthermore, *Six1*, *Runx1* and *Smad4* gene-dose-dependently activated ΔNp63 expression in MDE within vaginal fornix. Using a mouse model of diethylstilbestrol (DES)-associated vaginal adenosis, we found DES action through epithelial estrogen receptor α (ESR1) down-regulates SIX1 and RUNX1 in MDE within the vaginal fornix. This study establishes that the vaginal/ectocervical cell fate of MDE is regulated by a collaboration of multiple transcription factors including SMAD4, SIX1 and RUNX1, and the down-regulation of these key transcription factors leads to vaginal adenosis.

Author Summary

In embryogenesis, differentiation fate of cells is specified through constant communication between neighboring cells. In this study, we investigated the molecular mechanism of epithelial cell fate commitment in the lower female reproductive organs utilizing mouse genetic models. The cell fate of epithelial cells in the uterus, cervix and vagina is directed by signaling from mesenchymal cells. We

demonstrated that within the epithelial cells of the developing vagina, signals from mesenchymal cells are integrated into activities of transcription factors including SMAD4, RUNX1 and SIX1, which dose-dependently co-operate in the determination of vaginal epithelial cell fate. Disruption of these processes alters the cell fate from vaginal to uterine epithelium, resulting in a condition called vaginal adenosis, a putative precursor of vaginal adenocarcinoma. Women exposed to diethylstilbestrol (DES) in the womb have about 40 times the risk of developing vaginal adenocarcinoma. We determined that developmental exposure to DES induces vaginal adenosis by repressing SIX1 and RUNX1 through ESR1 in the epithelial cells. This discovery enhances the understanding of how early-life events, such as exposure to endocrine disruptors, causes vaginal adenosis, and thus may contribute to the prevention and therapeutic treatment of idiopathic vaginal adenocarcinoma.

INTRODUCTION

In mammals, the majority of female reproductive tract (FRT) develops from the Müllerian ducts (MDs) [1-3]. During embryogenesis, the MDs undergo a dynamic transformation from simple tubes consisting of homogeneous epithelium and mesenchyme into distinct organs, namely the oviduct, uterus, cervix and vagina [2, 4]. Classic tissue recombination studies have established that organ-specific mesenchyme induces the differentiation of MD epithelium (MDE) into epithelia with unique morphology and functions [5-7]. In the lower MD, epithelial cells are committed to become stratified squamous epithelium of ectocervix and vagina (together referred to as “vagina” hereafter), as the expression of ΔNp63 transcription factor is induced by vaginal mesenchyme [8-10]. In MDE of the developing vagina, the expression of ΔNp63 is activated by mesenchymal paracrine factors: bone morphogenetic protein (BMP) 4, activin A (ActA) and fibroblast growth factor (FGF) 7 or 10 [11, 12]. SMAD4 is essential for the activation of ΔNp63 in MDE, and this transcription factor binds on the 5’ sequence adjacent to the transcription start site (TSS) of ΔNp63 in future vaginal epithelium (VgE) but not in future uterine epithelium (UtE) [12]. This SMAD-dependent activation of the ΔNp63 locus requires runt-related transcription factor 1 (RUNX1), a co-transcription factor of SMADs. In MDE, the expression of RUNX1 is activated by ActA through a SMAD-independent mechanism [11]. In addition, activation of the mitogen-activated protein kinase (MAPK) pathway by FGF7/10-FGF receptor 2 IIIb (FGFR2IIIb) is essential for the activation of ΔNp63 locus in MDE [11]. BMP4-SMADs, ActA-RUNX1 and FGF7/10-MAPK pathways are independently required for the vaginal cell fate commitment of MDE, as inactivation of *Smad4*, *Runx1* or *Fgfr2* in MDE results in uterine epithelial differentiation of MDE within the vagina, which is a congenital epithelial lesion called vaginal adenosis [11, 12]. Nevertheless, once the ΔNp63 locus is activated in MDE, the transcriptional activity of the ΔNp63 locus is cell-autonomously maintained by ΔNp63 protein itself [12]. Hence, the identity of VgE is maintained independent of mesenchymal factors [7, 8].

In this study, we investigated the role of sine oculis homeobox homolog 1 (SIX1) in the cell fate commitment of VgE. In mammals, *SIX1* and other five *SIX* genes (*SIX2*–*6*) synergistically regulate the

developmental process in multiple organs, including inner ear, salivary gland, kidney, lung, and trachea [13, 14]. In mouse FRTs, *Six1* is enriched in the vagina compared to the uterus [12, 15]. However, its biological function in FRT remains unclear. Our current mouse genetic study reveals that SIX1 co-operates with RUNX1 and SMAD4 in the activation of the ΔNp63 locus in MDE as a downstream transcription factor of BMP4, ActA and FGF7/10 in MDE. The etiology of vaginal adenosis, the putative precursor to vaginal adenocarcinoma (VAC) is commonly associated with intrauterine exposure to estrogenic compounds, including diethylstilbestrol (DES) [16]. Our previous studies established that DES induces vaginal adenosis through inhibition of ΔNp63 expression in MDE. Our current study provides evidence that DES blocks the activation of ΔNp63 locus in future VgE by repressing SIX1 and RUNX1 through epithelial estrogen receptor α (ESR1). Such discoveries from our models may contribute to the prevention and therapeutic treatment of VACs, the etiology of which is currently unknown.

RESULTS

Expression patterns of SIX1 in neonatal FRTs.

ΔNp63α is the dominant isoform of the transcription factor encoded by *Trp63*/*TP63* in mouse/human VgE [10, 12]. To identify molecules that control epithelial cell fate in the lower FRT, we conducted microarray analysis of neonatal vagina and uterus from MDE-specific conditional KO (cKO) and conditional heterozygous (cHet, control) mice of *Trp63* [12]. In the analysis, *Six1* was more enriched in vaginae than uteri (1.02 Log2 fold-change, p = 0.0013) at postnatal day 2 (PD2), when induction of ΔNp63 expression is in progress in the vagina (Fig 1A). The expression level of *Six1* transcripts was not significantly different between *Trp63* cKO and cHET mice (Log2 cHET/cKO = -0.176, p = 0.23) (GSE44697) [12], indicating that SIX1 is not the target of TRP63. Immunoblotting confirmed the results of microarray: SIX1 protein was detected in vaginae but not in uteri and ovaries from PD2 C57BL/6J mice (Fig 1B).

Similarly to the expression of ΔNp63 in developing vagina, SIX1 expression progressed from posterior to anterior. At birth, SIX1 was expressed in the MDE of the lower vagina but not in the upper vagina and cervix, where RUNX1 already highlighted the future VgE (Fig 1C). By PD2, SIX1 expression extended to the cervix (Fig 1D), thus SIX1 and RUNX1 were co-expressed in the future VgE. There were substantial differences in the expression patterns of SIX1 and RUNX1 in neonatal FRTs. RUNX1 was concentrated in the MDE in the cervical canal and the upper-portion of vagina, and the expression was reduced in the posterior portion from the outer-wall of the fornix (Fig 1D, outer-wall of fornix is marked with white dotted-line), whereas SIX1 was expressed at a similar level in both inner and outer walls of the fornix (Fig 1D). In addition, RUNX1 in MDE was down-regulated upon expression of ΔNp63 (Fig 1E, white arrow) [12], whereas SIX1 expression persisted in ΔNp63 positive cells (Fig 1E, yellow arrow).

SIX1 is a downstream transcription factor of SMAD4.

SIX1 was expressed in the fornices of ΔNp63 cKO and cHET mice [12] at PD14, confirming that expression of SIX1 is independent of ΔNp63 (Fig 2A). In contrast, expression of SIX was SMAD4 dependent: *Smad4* cKO mice [12] completely lacked the expression of SIX1 in the entire MDE as assessed at PD2 (n = 5) (Fig 2B).

The absence of SIX1 in *Smad4* cKO mice suggested that SIX1 is the downstream transcription factor of BMP4-SMAD pathway. Therefore, *Bmp4* was knocked out in vaginal mesenchyme utilizing *Twist2*^{Cre} [17], and the effect on the expression of SIX1 in the lower Müllerian duct was assessed. Mesenchyme-specific *Bmp4* conditional KO (ms-cKO) was embryonic lethal. Hence, we collected pelvic organs from *Bmp4* conditional ms-cKO and ms-cHET mice at embryonic day 15.5, when most *Bmp4* ms-cKO embryos exhibited normal growth. At embryonic day 15.5 (Fig 2C), RUNX1 expression highlighted the anterior portion of MDE in both *Bmp4* ms-cKO and ms-cHET mice. On the other hand, SIX1 expression in MDE was low and mostly cytoplasmic at this age. Nevertheless, the SIX1 signal in MDE was higher in *Bmp4* ms-cHET mice compared to *Bmp4* ms-cKO mice (n=3 each, Fig 2D),

117 suggesting that BMP4 is a factor regulating SIX1 expression in FRT. However, the effect of loss of
118 BMP4 on SIX1 expression was not comparable to the loss of SMAD4. This might be due to
119 incomplete deletion of *Bmp4* or compensation by other BMP family members, as phosphorylation of
120 SMAD1/5/9 was still present in the MDE of *Bmp4* cKO mice (Fig 2C).
121
122 **ActA-RUNX1 and FGF7/10-MAPK pathways positively regulate SIX1 in MDE**
123 Although SIX was expressed throughout the VgE in *Runx1* cKO mice [12] (Fig 3A), the expression of
124 SIX1 in the fornix was significantly reduced compared to *Runx1* cHET mice (Fig 3B and 3C). Thus,
125 the expression level of SIX1 in MDE is positively regulated by ActA-RUNX1 signaling activity. Similarly,
126 SIX1 expression was slightly reduced in the fornix of *Fgfr2* cKO mice [11] (Fig 3D). However, SIX1
127 expression in the fornix was uniformly up-regulated when the vaginal defect of *Fgfr2* cKO MDE was
128 corrected with the expression of a constitutively active MAP2K1 ($MAP2K1^{DD}$) [11] (Fig 3D and 3E),
129 suggesting that MAPK activity modulates the expression level of SIX1 protein in the vaginal fornix.
130 Accordingly, we tested the effect of BMP4, ActA and FGF10 on SIX1 expression in uterine organ
131 culture assay. ActA and FGF10 had minimal to no effect on SIX1 expression in the epithelium of
132 uterine explants (not shown). BMP4 slightly increased SIX1 in UtE, but the nuclear expression was
133 mostly absent (Fig 3F). Even when all 3 factors were combined, nuclear SIX1 expression was
134 detected only in portions of UtE showing ΔNp63 expression, suggesting that SIX1 promotes ΔNp63
135 expression in MDE. In the uterine organ culture, growth factors in the medium must diffuse through
136 the mesenchymal layers to act on UtE. Diffusion of FGF10 within connective tissues is limited
137 because of its high affinity to heparan sulfate [18]. Accordingly, we replaced FGF10 with the
138 expression of $MAP2K1^{DD}$, which itself did not induce expression of ΔNp63, RUNX1 and SIX1 [11].
139 ActA and BMP4 efficiently induced SIX1 as well as ΔNp63 in *Map2k1*^{DD} transgenic UtE (Fig 3F and
140 3G) indicating that SIX1 is the downstream transcription factor of BMP4-SMAD, ActA-RUNX1 and
141 FGF7/10-MAPK in MDE.
142

143 **_Six1_ and _Runx1_ dose-dependently promote ΔNp63 expression in MDE**

144 Since Six1 null mice die before vaginal epithelial differentiation occurs [19], the role of SIX1 in VgE
145 differentiation was assessed by genetically inactivating *Six1* in MDE by *Wnt7a-Cre* [20]. *Six1* cKO
146 mice were born with the expected Mendelian ratio demonstrating no gross abnormality. However, loss
147 of SIX1 in MDE affected the formation of ΔNp63-positive basal epithelial layer in the vaginal fornix,
148 and a substantial area of epithelium was negative for ΔNp63-positive cells at PD4 (Fig 4A). Thus,
149 SIX1 is one of key transcription factors that mediate the paracrine mesenchymal signaling in the
150 vaginal cell fate commitment of MDE. Nevertheless, the defect of *Six1* cKO vagina was relatively
151 minor, and a continuous ΔNp63 positive layer formed in the fornix by PD14, as the lateral growth of
152 ΔNp63 positive cells filled the gaps (not shown). The distinctive vaginal phenotypes of *Six1* cKO mice
153 from *Smad4*, *Runx1* and *Fgfr2* cKO mice indicate that SIX1 is only one of many downstream factors
154 mediating signaling from mesenchymal cells in MDE. While *Smad4*, *Runx1* and *Fgfr2* cKO mice lost
155 ΔNp63 expression in MDE within the entire (*Smad4*, and *Fgfr2* cKO) or upper (*Runx1* cKO) vagina,
156 the vaginal defect of *Six1* cKO mice was restricted to the epithelium on the outer-wall of vaginal fornix,
157 where the expression of RUNX1 is reduced (Fig 1D). Meanwhile, RUNX1 expression in the vaginal
158 fornix was not affected in *Six1* cKO mice (Fig 4A). Hence, we generated the compound conditional
159 mutant mice of *Six1* and *Runx1* to assess if SIX1 and RUNX1 collaborate in the ΔNp63 expression of
160 MDE in the outer-wall of vaginal fornix. Monoallelic loss of *Runx1* in MDE exaggerated the effect of
161 *Six1* alleleic loss on ΔNp63 expression: While monoallelic loss (cHET) of *Six1* or *Runx1* alone had no
162 evident effect on the formation of ΔNp63-positive basal layer, the *Six1;Runx1* double cHET mice had
163 a significantly reduced number of ΔNp63-positive basal cells in the outer-wall of fornix (Fig 4B and
164 4C). The ΔNp63-negative epithelial area expanded further to the inner wall of fornix when biallelic loss
165 (cKO) of *Six1* was combined with monoallelic loss of *Runx1* (Fig 4B and 4C). The differentiation of
166 MDE itself was not retarded in the mutant mice, as ΔNp63 negative MDE expressed progesterone
167 receptor (PGR), indicating uterine cell fate commitment [21] (Fig 4D).
168

Gene-dose-dependent function of *Six1*, *Runx1* and *Smad4* in activation of ΔNp63 locus in MDE.

The distinctive vaginal phenotypes of *Six1* cKO and *Smad4* cKO mice indicate that SMAD4 works independent of SIX1 in vaginal cell fate commitment of MDE. Accordingly, we assessed if the efficacy of SIX1 and RUNX1 in the activation ΔNp63 expression in MDE is affected by monoallelic loss of *Smad4* gene, which alone does not block the formation of ΔNp63-positive basal layer in VgE [12]. *Six1;Smad4* double cHET mice expressed ΔNp63 throughout the vagina at PD4. However, the density of basal cells on the outer-wall of the fornix was reduced (Fig 5). The synergy between *Six1* and *Smad4* alleles became more prominent when an additional *Six1* allele was inactivated (Fig 5). Similarly, monoallelic loss of *Smad4* and *Runx1* synergistically affected the density of ΔNp63 in the fornix. Accordingly, *Six1;Smad4;Runx1* triple cHET mice demonstrated gaps in the ΔNp63-positive basal layer throughout the vaginal fornix (Fig 5). The effect of monoallelic *Smad4* loss on the density of TRP63 positive cells was statistically significant in mice with certain genotypes (Table 1). For instance, TRP63-positive cell density in the outer and inner fornix walls of *Six1* cHET mice was not significantly different from that in WT mice. However, the TRP63-positive cell density in *Six1* cHET mice became significantly lower with the monoallelic loss of *Smad4* (*Six1* cHET; *Smad4* cHET) compared to WT mice (Fig 5 B and C).

Table 1. One-way ANOVA followed by Tukey's multiple comparison test of TRP63-posittive cell density in the outer and inner vaginal fornix walls of *Six1*, *Runx1*, *Smad4* compound mutant mice.

188

Outer wall

			Smad4 WT							*Smad4* HET				
			Runx1 WT			*Runx1* HET			*Runx1* KO	*Runx1* WT			*Runx1* HET	
		Six1	WT	HET	KO	WT	HET	KO	WT	WT	HET	KO	WT	HET
Smad4 WT	*Runx1* WT	WT		NS	p<0.01	NS	p<0.01	p<0.01	p<0.01	NS	p<0.01	p<0.01	p<0.01	p<0.01
		HET			NS	NS	p<0.05	p<0.01	p<0.01	NS	NS	p<0.01	NS	p<0.01
		KO				NS	NS	NS	p<0.01	NS	NS	NS	NS	p<0.01
	Runx1 HET	WT					p<0.05	p<0.01	p<0.01	NS	NS	p<0.01	NS	p<0.01
		HET						NS	p<0.05	p<0.01	NS	NS	NS	NS
		KO							NS	p<0.01	NS	NS	NS	NS
	Runx1 KO	WT								p<0.01	p<0.01	NS	p<0.01	NS
Smad4 HET	*Runx1* WT	WT									NS	p<0.01	p<0.05	p<0.01
		HET										NS	NS	p<0.01
		KO											NS	NS
	Runx1 HET	WT												p<0.01
		HET												

189

Inner wall

			Smad4 WT							*Smad4* HET				
			Runx1 WT			*Runx1* HET			*Runx1* KO	*Runx1* WT			*Runx1* HET	
		Six1	WT	HET	KO	WT	HET	KO	WT	WT	HET	KO	WT	HET
Smad4 WT	*Runx1* WT	WT		NS	NS	NS	p<0.01	p<0.01	p<0.01	NS	p<0.01	p<0.01	NS	p<0.01
		HET			NS	NS	NS	p<0.01	p<0.01	NS	NS	NS	NS	p<0.01
		KO				NS	NS	p<0.05	p<0.01	NS	NS	NS	NS	p<0.05
	Runx1 HET	WT					NS	p<0.01	p<0.01	NS	NS	p<0.05	NS	p<0.01
		HET						NS	p<0.01	NS	NS	NS	NS	NS
		KO							p<0.01	p<0.05	NS	NS	p<0.05	NS
	Runx1 KO	WT								p<0.01	p<0.01	p<0.01	p<0.01	p<0.01
Smad4 HET	*Runx1* WT	WT									NS	NS	NS	p<0.01
		HET										NS	NS	NS
		KO											NS	NS
	Runx1 HET	WT												p<0.01
		HET												

190

NS: not significant

Regulatory elements of ΔNp63

The gene-dose-dependent effect of *Six1, Runx1* and *Smad4* on ΔNp63 activation suggests collaboration between these transcription factors in the vaginal cell fate commitment of MDE. The analysis of evolutionally conserved regions by ECR browser [22] identified numerous numbers of putative enhancer elements within *TP63*/*Trp63* locus. Many of these conserved sequences near ΔNp63 TSS contained binding sites for SMADs, RUNX1 as well as SIX1 (S1 Fig). The 5' sequence proximal to ΔNp63 TSS, to which SMAD4 binds in VgE but not UtE, also contained binding sites of SMAD4, RUNX1 and SIX1 (S2A Fig). Thus, we genetically tested if the putative 5' proximal enhancer and the promoter (mm10 Chr16: 25801055-25802045) are sufficient to replicate the expression patterns of ΔNp63 by generating transgenic mice (S2 Fig). However, the transgene (Cre-ires-EGFP) was not expressed in any tissues of 5 founders of transgenic mice. Furthermore, the progenies of the founders carrying *ROSA*$^{mT\text{-}mE}$ [23] and ΔNp63-Cre-ires-EGFP alleles were also totally negative for EGFP/mEGFP (not shown), indicating the insufficiency of the sequence by itself to replicate the expression patterns of ΔNp63 in MDE. Surprisingly, ΔNp63-Cre knock-in (KI) mice, in which the coding sequence in the first exon of ΔNp63 was replaced with Cre [24] also failed to express the Cre transgene in VgE: When ΔNp63-Cre KI mice were crossed with *ROSA*$^{mT\text{-}mE}$ reporter mice, the most epithelial cells in vagina of *ROSA*$^{mT\text{-}mE}$;*ΔNp63-Cre* KI double-transgenic mice were negative for mEGFP (n=3, S2C Fig). ConTra v3 analysis [25] identified conserved binding sites of SMAD1, SMAD4 and RUNX1 in the sequence deleted in the genome of ΔNp63-Cre KI mice (S1E Fig). Thus, the efficient activation of ΔNp63 locus in MDE appeared to require cooperation of multiple regulatory elements including the protein coding sequence within exon 1. Notably, conserved binding sites of SIX1, RUNX1 and SMADs were not always clustered together, suggesting that these transcription factors may independently act on different enhancer elements. Thus, the gene-dose effects of *Six1*, *Runx1* and *Smad4* on ΔNp63 activation may reflect the number of active enhancer-like elements that cooperate in the remodeling of ΔNp63 locus.

Diethylstilbestrol (DES) inhibits activation of ΔNp63 locus in MDE through down-regulation of RUNX1 and SIX1.

Previously, we demonstrated that down-regulation of RUNX1 is involved in the pathogenesis of DES-associated vaginal adenosis. DES down-regulated RUNX1 in MDE of vaginal fornix within 24 hours (Fig 6A). However, the effect of 24-hour DES-treatment was more prominent on SIX1 than RUNX1: Nuclear expression of SIX1 disappeared from the MDE in the vaginal fornix and the cervical canal of DES-treated mice (Fig 6A and 6B). DES slightly reduced pSMAD1/5/9 in the vaginal mesenchyme, while DES had no evident effect on the epithelial pSMAD1/5/9 (Fig 6C). In contrast, DES-treatment consistently increased MAPK1/3 activity in vaginal epithelium and mesenchyme (Fig 6C). Hence, the down-regulation of SIX1 was not likely due to the repression of BMP4 or FGF7/10 activity in MDE by DES.

Our previous tissue recombination study has established that DES blocks expression of ΔNp63 in MDE through estrogen receptor α (ESR1) within epithelial cells [4, 8]. The expression patterns of SIX1, RUNX1 and ΔNp63 in the fornix of *Esr1* cKO mice were indistinguishable from these in wild type mice at PD3 (Fig 7A). In agreement with the tissue recombination study, DES did not block the induction of ΔNp63 in the VgE when *Esr1* was deleted in MDE by *Wnt7a-Cre* (*Esr1* cKO mice) (Fig 7B). Moreover, DES exposure promoted the expression of ΔNp63 in VgE in *Esr1* cKO mice (Fig 7B), forming a continuous layer of ΔNp63-positive cells by PD3, ≥ 1 day earlier than normal development. Therefore, ESR1 in epithelium and mesenchyme has the opposite effect on the induction of ΔNp63 (S3 Fig). In fact, DES-treatment induced RUNX1 and SIX1 in the UtE of *Esr1* cKO mice by PD3 (not shown).

DES-ESR1 activity attenuates the expression of SIX1 and RUNX1 in MDE cell-autonomously, as the expression of SIX1 and RUNX1 was maintained in the vaginal fornices of *Esr1* cKO mice (Fig 7C). Interestingly, the effect of DES on MAPK1/3 activity in MDE and mesenchyme was exaggerated in the vagina of *Esr1* cKO mice (Fig 7C), indicating that epithelial ESR1 repressed the FGF7/10-MAPK1/3 signaling pathway in both vaginal epithelium and mesenchyme. A continuous layer of ΔNp63-positive basal cells formed by PD3 on the outer wall of vaginal fornix in MAP2K1^{DD} conditional transgenic mice

(Fig 7D, control), suggesting that DES promotes vaginal differentiation of MDE by activating the MAPK pathway. Nevertheless, DES repressed the expression of SIX1 and ΔNp63 in MDE expressing $MAP2K1^{DD}$ (Fig 7D, DES). Thus, the activation of MAPK pathway alone did not protect MDE from DES-induced vaginal adenosis.

DISCUSSION

It has long been known that the differentiation of MDE into distinctive epithelia of uterus and vagina is under the control of organ-specific mesenchyme [5]. Through a series of studies with genetically engineered mice, our group has established that ΔNp63 is the master regulator of vaginal epithelial differentiation in MDE [8], and that the expression of ΔNp63 is induced by mesenchymal paracrine factors, BMP4, ActA and FGF7/10 [11, 12]. Within MDE, the signals from underlying mesenchyme are transduced by BMP4-SMADs, ActA-RUNX1 and FGFs-MAPKs. Since mouse vaginal mesenchyme can induce ΔNp63 and squamous differentiation in human MDE, the molecules that mediate the communication between mesenchyme and epithelium in the commitment of MDE to vaginal cell fate must be common between these two species [26].

In this study, we identified SIX1 as a key transcription factor that mediates the mesenchymal signals in the activation of ΔNp63 locus during vaginal cell fate commitment of MDE. Subsequently, we propose that vaginal mesenchymal factors induce MDE to commit to vaginal epithelial cell fate by activating ΔNp63 locus through cooperation of multiple enhancer elements, which are activated by SMADs, RUNX1 and/or SIX1 (Fig. 8). An enhancer is a genomic region of few hundred base pairs that contains clustered binding-sites for multiple transcription factors. Although many transcription factors cannot bind their target site in the context of nucleosomal DNA, enhancer-mediated simultaneous-binding of multiple transcription factors can overcome the nucleosome barrier [27]. Thus, enhancers integrate multiple signaling pathways through binding of downstream effectors [28, 29]. In cell fate commitment of MDE to VgE, BMP, ActA and FGF pathways are integrated to prime VgE-specific gene expression programs in MDE through the simultaneous binding of SMADs, RUNX1 and

SIX1 to ΔNp63 enhancers (Fig. 8). Approximately 80% of all characterized mouse enhancers show tissue-specific expression [30]. In this regard, the enhancers that regulate ΔNp63 expression in MDE must be distinctive from those in the skin because *Six1* null [19] and *Runx1* null [31] mice do not exhibit the deformation of skin and appendages observed in ΔNp63 mutant mice [32]. The identification of key regulator elements of ΔNp63 in MDE is imperative to fully appreciate the pathogenesis of vaginal adenosis, which is a result of faulty cell fate commitment of VgE. However, enhancers can regulate the expression of genes that are mega-bases apart [30, 33]. Therefore, the identification of key regulator elements of ΔNp63 in MDE requires genome-wide screening of transcription factor binding sites by chromatin immunoprecipitation-sequencing (ChIP-seq). However, the usage of ΔNp63 enhancers must be unique between different regions of MDE as demonstrated by the difference in the requirement of SMAD4, RUNX1 and SIX1 for ΔNp63 expression in mouse genetic studies. Given the heterogeneity of the cell population, the narrow developmental time window, and the small tissue amount of MDE, the identification of ΔNp63 regulatory elements in MDE by current standard techniques is challenging.

Most vaginal adenocarcinomas (VACs) are believed to arise from vaginal adenosis because of the presence of adenosis lesions at the primary site of VACs. Hence, better understanding in etiology of vaginal adenosis is particularly crucial in order to develop preventive and therapeutic approaches for VACs. In the past, *in utero* DES-exposure was the primary cause of vaginal adenosis and VAC. Since the expression patterns of ΔNp63 and RUNX1 as well as the effect of DES on the expression of these transcription factors are identical between human and mouse MDE [1, 10, 26, 34], the molecular model established in mice (Fig 8) should explain the etiology of vaginal adenosis in DES-exposed women. However, VACs occur in women who have no history of DES exposure [16, 35]. Because the expression of ΔNp63 in the lower MDE occurs during the first trimester in human fetus [10, 34], the pathogenesis of non-DES-associated VACs should still involve an *in utero* event that disturbs the vaginal epithelial cell fate commitment in MDE. In this regard, exposure to a compound that inhibits any pathways/molecules described in Fig 8 can lead to vaginal adenosis. As cell fate commitment of

mouse VgE occurs in the first week of postnatal development [3, 10], neonatal mice would be useful to screen medical and environmental chemicals that interfere ΔNp63 expression in VgE.

Some studies suggest the *de novo* formation of adenosis in the vagina of adult women associated with medical treatments [36-38]. However, given the low detection sensitivity of routine colposcopy and cytology screenings for adenosis, adenosis cases that appear to be *de novo* are likely due to an increased visibility of previously imperceptible adenosis lesions enlarged by a reactive change to medical treatments.

In addition to vaginal adenosis, perinatal DES exposure of female mice induces uterine squamous metaplasia [39], a formation of squamous epithelium within the simple columnar UtE. Interestingly, the gene expression pattern of uterine squamous metaplasia lesions is identical to that of normal VgE [4, 8], indicating that uterine squamous metaplasia is vaginal cell fate commitment of MDE within the uterus. Thus, developmental DES exposure elicits opposite effects on the cell fate commitment of MDE in developing uterus versus vagina. This intriguing dual-effect of DES is explained by the opposite functions of epithelial versus mesenchymal ESR1. As shown in our current study, DES action through epithelial ESR1 interferes the activation of ΔNp63 locus whereas DES action through mesenchymal ESR1 promotes ΔNp63 expression (S3 Fig). When ESR1 is expressed in both epithelium and mesenchyme, DES effects via epithelial ESR1 are dominant. In developing uterus and vagina, ESR1 is initially expressed only in mesenchymal cells, and ESR1 expression in MDE occurs at the posterior end and gradually progresses anterior [7, 34]. DES exposure most efficiently induces vaginal adenosis at the first trimester of human fetuses and the postnatal day 1- 5 in neonatal mice, when ESR1 is expressed in the MDE of the vagina but not the uterus. Accordingly, DES blocks ΔNp63 activation in the vagina through epithelial ESR1 and activates ΔNp63 in the uterus through mesenchymal ESR1. Our current study predicts that DES induces expression of BMPs, FGFs and Activin/TGFβ through ESR1 in the uterine mesenchyme. On the other hand, molecular mechanisms through which DES represses RUNX1 and SIX1 in MDE remain unclear. Elucidating the underlying

molecular pathogenesis of DES-associated adenosis will help identify etiology of non-DES-associated vaginal adenosis and VAC.

METHODS

Mouse models

All animal procedures were approved by the Animal Care and Use Committee in the Ohio State University. The mouse strains carrying the following alleles were utilized: *Six1*^{flox} [*Six1*$^{tm2.1Mair}$] [40], *Trp63*^{flox} [*Trp63*$^{tm3.2Brd}$] [41], ΔNp63-EGFP knock-in (*Trp63* $^{\Delta Np63\text{-}EGFP\text{-}KI}$) [32], *Runx1*^{flox} [*Runx1*^{tm1Tani}] [42], *Fgfr2*^{flox} [*Fgfr2*^{tm1Dor}*/J*] [43], *ROSA*$^{mT\text{-}mE}$ [*Gt(ROSA)26Sor*$^{tm4(ACTB\text{-}tdTomato,\text{–}EGFP)Luo}$*/J*] [23], *ROSA*^{MAP2K1DD} [*Gt(ROSA)26Sor*$^{tm8(Map2k1*,EGFP)Rsky}$*/J*] [44], *Smad4*^{flox} (*Smad4*$^{tm2.1Cxd}$*/J*) [45], *Esr1*^{flox} [46], *Bmp4*^{flox} [*Bmp4*^{tm1Jfm}] [47], *Twist2*^{Cre} [*Twist2*$^{tm1.1(cre)Dor}$] [17], *Pax2-Cre* [Tg(Pax2-cre)1Akg] (MMRRC) [48], *Wnt7a-Cre* [20] and ΔNp63-Cre [*Trp63*$^{tm1.1(cre)Ssig}$*/J*] [24]. C57BL/6J mice were purchased from Jackson Laboratory (Bar Harbor, ME). MDE-specific conditional knockout (cKO) and conditional heterozygous (cHET) mice were generated by crossing lines carrying floxed alleles with *Wnt7a-Cre* mice, except for *Trp63*^{flox} mice, which were crossed with *Pax2-Cre*. *Twist2*^{Cre} mice were used for mesenchyme-specific deletion of *Bmp4*. The day of birth was count as PD1.

Neonatal DES treatment

A ~40 μg DES slow-release pellet was prepared as previously described [12]. The ~0.04 mg/mm DES filled tubing was cut into 1 mm length and subcutaneously injected into newborn mice using a 19 gauge trocar.

Immunofluorescence (IF) and immunohistochemistry (IHC)

IF and IHC assays were performed as previously described [49]. Briefly, tissues were fixed with Modified Davidson's fixative solution (Electron Microscopy Sciences, Hatfield, PA), processed into paraffin, and sectioned at 5 μm. The sections were heated in 10 mM sodium citrate buffer (pH 6.0) containing 0.05% Tween-20 for 35 min in an Electric Pressure Cooker. The following primary antibodies were used at the indicated dilutions: anti-CTNNB1 (CAT-5H10) (1:100, 13-8400) from ThermoFisher (Waltham, MA); anti-TRP63 (4A4) (1:200, 790-4509) from Ventana Medical Systems (Tucson, AZ); anti-ΔNp63 (1:2,000, PC373) from Millipore (Billerica, MA); anti-PGR (1:200, A0098) from Agilent Technologies (Santa Clara, CA); anti-RUNX1 (2593-1, 1:400) from Epitomics (Burlingame, CA); anti-phospho (p)-MAPK1/3 (p-T202/Y201, 1:30, #4370) and anti-pSMAD1/5/9 (1:50, #9511) from Cell Signaling Technology (Danvers, MA); anti-GFP (1:100, ab6673) from Abcam (Cambridge, MA); anti-SIX1 (1:800, HPA001893) from Sigma-Aldrich (St. Louis, MO); anti-ESR1 (1:100, RM-9101) from Lab Vision (Fremont, CA). For IF assay, Alexa-Fluor594 anti-mouse IgG (H+L) (1:1,000, 715-586-150) and Alexa-Fluor488 anti-rabbit IgG (H+L) (1:1,000, 711-546-152) from Jackson ImmunoResearch (West Grove, PA) were used for the secondary antibodies, and bisbenzimide H 33258 (Hoechst 33258, 1:10,000, Sigma-Aldrich) was used for nuclear staining. For IHC with DAB (3,3'-diaminobenzidine, Sigma-Aldrich), biotinylated anti-rat IgG (H+L) (1:800, 712-066-153) was used in conjunction with streptavidin-horseradish peroxidase (1:400, 016-030-084, Jackson ImmunoResearch). Micrographs were captured using a BZ-9000 microscope (Keyence, Osaka, Japan) under identical conditions between samples for each antibody. The contrast of images was adjusted by applying identical parameters to the images for each antibody with the batch-process function of Adobe Photoshop CS6 (Adobe, CA, San Jose, CA, USA). To capture a wide area in a single image, tissue sections were scanned in multiple frames, and the images were automatically merged together utilizing the Image Stitching function of image analysis tool.

Morphometric analysis

The methods for the quantitative analysis on the squamous transformation of MDE [12] and the IF signal [50] were previously described. We adapted these methods with some modifications. The length of epithelium at the basal lamina was measured in the outer-wall of vaginal fornix in at least 2 sections per animal in TRP63 immunostained sections. The proportion of epithelium with ΔNp63-psotive basal layer was calculated by "length of epithelial basement membrane associated with TRP63-positive cells" ÷ "total epithelial basement membrane length" x 100, for each mouse.

Basal cell density in the outer and inner fornix walls was calculated by number of TRP63-positive pixels per epithelial basement membrane length. In tissue sections of vaginal fornices stained for TRP63, epithelial areas were manually selected, and the pixels positive for TRP63 signal within the epithelium were selected by adjusting the lower threshold for positivity to exclude background noise. Epithelial basement membrane was manually marked on the IF images, and the p63-positive area and the basement membrane length were measured utilizing Image J (NIH, Bethesda, MD). Analysis was performed on ≥ 4 fornice from ≥ 3 mice per group. The value in each fornix was considered as a single measurement. Statistical significance was analyzed by One-way ANOVA with post-hoc Tukey's HSD Test.

SIX1 IF analysis

Quantitative IF assay was performed as previously described with modifications [50]. Tissue sections for an analysis were stained together, and images were captured at the same time under the identical conditions. Images of ≥ 4 tissue sections from n≥ 3 independent animals were analyzed for each group. Epithelial areas were manually selected, and the signal intensity per pixel within the epithelial area was measured by Image J. In all experiments, approximately equivalent areas were analyzed in each sample, and there was no significant intragroup difference in the average signal intensity. Thus, all samples in each group were plotted together, and the distributions of signals were compared between groups by the Mann–Whitney U test with continuity correction.

394

395 **Immunoblot analysis**

396 Ovaries, uteri and vaginae from PD2 mice (5- 6 mice per blot) were homogenized with a minipestle in
397 ice-cold lysis buffer containing protease (cOmplete Protease Inhibitor Cocktail,Roche) and
398 phosphatase (phoSTOP, Roche) inhibitors and loaded onto NuPAGE 4–12% Bis-Tris precast SDS-
399 PAGE gel. Proteins were transferred to a PVDF membrane (Millipore Sigma, St. Louis, MO, USA).
400 The membrane was incubated with anti-RUNX1 antibody (1: 2000, Epitomics), anti-SIX1 antibody
401 (1:1,000, Millipore Sigma) and GAPDH (1: 2000, G8795, Millipore Sigma) in the OdysseyR Blocking
402 buffer (TBS) (from LI-COR Biosciences, NE, USA) overnight at 4 °C. IRDye® 800CW Donkey anti-
403 rabbit IgG, IRDye® 680LT Donkey anti-rabbit IgG and IRDye® 680LT Donkey anti-mouse IgG were
404 used for the secondary antibodies. The signal was detected using Odyssey CLx Imaging System (LI-
405 COR Biosciences, NE, USA). The analysis was repeated 3 times with independent samples.

406

407 **Uterine organ culture**

408 Uterine hanging drop organ culture was performed as previously described with minor modifications
409 [11]. Briefly, uteri were dissected from PD1 mice, cleaned by removing connective tissues, and cut
410 into 3 pieces per uterine-horn in Dulbecco's Modified Eagle Medium/Nutrient Mixture F-12
411 (DMEM/F12, 11039, Life Technologies) containing 10 nM ICI 182,780 (Sigma-Aldrich). The uterine
412 pieces were then placed in autoclaved PCR tube caps (AXYGEN, Union City, CA) with basal medium
413 (10 nM ICI 182,780 DMEM/F12 with Insulin-Transferrin-Selenium and Antibiotic-Antimycotic)
414 with/without 20 ng/ml human recombinant BMP4, ActA and/or FGF10 (Life Technologies), inverted,
415 and incubated. Uterine pieces were cultured up to 3 days with daily medium change, fixed with
416 Modified Davidson's fixative, and processed for histological analysis.

417

418 **ACKNOWLEDGMENTS**

The authors thank Dr. Altea Rocci, Shayna Wallace, Justin Thomas and the Solid Tumor Biology Research group histology core for technical help. This work was supported by the National Institutes of Health [RO1CA154358, RO1HD064402, P30CA016058 to T.K.].

REFERENCES

1. Robboy SJ, Kurita T, Baskin L, Cunha GR. New insights into human female reproductive tract development. Differentiation; research in biological diversity. 2017;97:9-22. doi: 10.1016/j.diff.2017.08.002. PubMed PMID: 28918284.

2. Kurita T. Developmental origin of vaginal epithelium. Differentiation; research in biological diversity. 2010;80(2-3):99-105. Epub 2010/07/20. doi: 10.1016/j.diff.2010.06.007. PubMed PMID: 20638775; PubMed Central PMCID: PMC2943051.

3. Kurita T, Nakamura H. Embryology of the uterus. In: Aplin JD, Fazleabas AT, Glasser SR, Giudice LC, editors. Endometrium. 2 ed. London, UK: Informa UK Ltd.; 2008. p. 1-18.

4. Kurita T. Normal and abnormal epithelial differentiation in the female reproductive tract. Differentiation; research in biological diversity. 2011;82(3):117-26. Epub 2011/05/27. doi: 10.1016/j.diff.2011.04.008. PubMed PMID: 21612855; PubMed Central PMCID: PMC3178098.

5. Cunha GR. Stromal induction and specification of morphogenesis and cytodifferentiation of the epithelia of the Müllerian ducts and urogenital sinus during development of the uterus and vagina in mice. The Journal of experimental zoology. 1976;196(3):361-70. PubMed PMID: 932664.

6. Boutin E, Sanderson R, Bernfield M, Cunha GR. Expression of syndecan, a cell surface proteoglycan, correlates with induced changes in cellular organization. The Journal of cell biology. 1989;107:605a.

7. Kurita T, Cooke PS, Cunha GR. Epithelial-stromal tissue interaction in paramesonephric (Mullerian) epithelial differentiation. Developmental biology. 2001;240(1):194-211. Epub 2002/01/11. doi: 10.1006/dbio.2001.0458. PubMed PMID: 11784056.

445 8. Kurita T, Mills AA, Cunha GR. Roles of p63 in the diethylstilbestrol-induced cervicovaginal
446 adenosis. Development (Cambridge, England). 2004;131(7):1639-49. Epub 2004/03/05. doi:
447 10.1242/dev.01038. PubMed PMID: 14998922.
448 9. Kurita T, Cunha GR. Roles of p63 in differentiation of Mullerian duct epithelial cells. Annals of
449 the New York Academy of Sciences. 2001;948:9-12. Epub 2002/01/25. PubMed PMID: 11795399.
450 10. Kurita T, Cunha GR, Robboy SJ, Mills AA, Medina RT. Differential expression of p63 isoforms
451 in female reproductive organs. Mechanisms of development. 2005;122(9):1043-55. Epub 2005/06/01.
452 doi: 10.1016/j.mod.2005.04.008. PubMed PMID: 15922574.
453 11. Terakawa J, Rocchi A, Serna VA, Bottinger EP, Graff JM, Kurita T. FGFR2IIIb-MAPK activity
454 is required for epithelial cell fate decision in the lower Mullerian duct. Molecular endocrinology
455 (Baltimore, Md. 2016:me20161027. doi: 10.1210/me.2016-1027. PubMed PMID: 27164167.
456 12. Laronda MM, Unno K, Ishi K, Serna VA, Butler LM, Mills AA, et al. Diethylstilbestrol induces
457 vaginal adenosis by disrupting SMAD/RUNX1-mediated cell fate decision in the Mullerian duct
458 epithelium. Developmental biology. 2013;381(1):5-16. Epub 2013/07/09. doi:
459 10.1016/j.ydbio.2013.06.024. PubMed PMID: 23830984.
460 13. Kawakami K, Sato S, Ozaki H, Ikeda K. Six family genes--structure and function as
461 transcription factors and their roles in development. Bioessays. 2000;22(7):616-26. doi:
462 10.1002/1521-1878(200007)22:7<616::AID-BIES4>3.0.CO;2-R. PubMed PMID: 10878574.
463 14. Kochhar A, Fischer SM, Kimberling WJ, Smith RJ. Branchio-oto-renal syndrome. Am J Med
464 Genet A. 2007;143A(14):1671-8. doi: 10.1002/ajmg.a.31561. PubMed PMID: 17238186.
465 15. Jefferson WN, Chevalier DM, Phelps JY, Cantor AM, Padilla-Banks E, Newbold RR, et al.
466 Persistently altered epigenetic marks in the mouse uterus after neonatal estrogen exposure.
467 Molecular endocrinology (Baltimore, Md. 2013;27(10):1666-77. doi: 10.1210/me.2013-1211. PubMed
468 PMID: 24002655; PubMed Central PMCID: PMC3787132.
469 16. Laronda MM, Unno K, Butler LM, Kurita T. The development of cervical and vaginal adenosis
470 as a result of diethylstilbestrol exposure in utero. Differentiation; research in biological diversity.

2012;84(3):252-60. Epub 2012/06/12. doi: 10.1016/j.diff.2012.05.004. PubMed PMID: 22682699; PubMed Central PMCID: PMC3443265.

17. Sosic D, Richardson JA, Yu K, Ornitz DM, Olson EN. Twist regulates cytokine gene expression through a negative feedback loop that represses NF-kappaB activity. Cell. 2003;112(2):169-80. PubMed PMID: 12553906.

18. Izvolsky KI, Shoykhet D, Yang Y, Yu Q, Nugent MA, Cardoso WV. Heparan sulfate-FGF10 interactions during lung morphogenesis. Developmental biology. 2003;258(1):185-200. PubMed PMID: 12781692.

19. Laclef C, Hamard G, Demignon J, Souil E, Houbron C, Maire P. Altered myogenesis in Six1-deficient mice. Development (Cambridge, England). 2003;130(10):2239-52. PubMed PMID: 12668636.

20. Winuthayanon W, Hewitt SC, Orvis GD, Behringer RR, Korach KS. Uterine epithelial estrogen receptor alpha is dispensable for proliferation but essential for complete biological and biochemical responses. Proceedings of the National Academy of Sciences of the United States of America. 2010;107(45):19272-7. Epub 2010/10/27. doi: 10.1073/pnas.1013226107. PubMed PMID: 20974921; PubMed Central PMCID: PMC2984169.

21. Kurita T, Lee KJ, Cooke PS, Taylor JA, Lubahn DB, Cunha GR. Paracrine regulation of epithelial progesterone receptor by estradiol in the mouse female reproductive tract. Biology of reproduction. 2000;62(4):821-30. Epub 2000/03/22. PubMed PMID: 10727249.

22. Ovcharenko I, Nobrega MA, Loots GG, Stubbs L. ECR Browser: a tool for visualizing and accessing data from comparisons of multiple vertebrate genomes. Nucleic acids research. 2004;32(Web Server issue):W280-6. doi: 10.1093/nar/gkh355. PubMed PMID: 15215395; PubMed Central PMCID: PMC441493.

23. Muzumdar MD, Tasic B, Miyamichi K, Li L, Luo L. A global double-fluorescent Cre reporter mouse. Genesis. 2007;45(9):593-605. PubMed PMID: 17868096.

24. Pignon JC, Grisanzio C, Geng Y, Song J, Shivdasani RA, Signoretti S. p63-expressing cells are the stem cells of developing prostate, bladder, and colorectal epithelia. Proceedings of the

National Academy of Sciences of the United States of America. 2013;110(20):8105-10. doi: 10.1073/pnas.1221216110. PubMed PMID: 23620512; PubMed Central PMCID: PMC3657776.

25. Kreft L, Soete A, Hulpiau P, Botzki A, Saeys Y, De Bleser P. ConTra v3: a tool to identify transcription factor binding sites across species, update 2017. Nucleic acids research. 2017;45(W1):W490-W4. doi: 10.1093/nar/gkx376. PubMed PMID: 28472390; PubMed Central PMCID: PMC5570180.

26. Cunha GR, Kurita T, Cao M, Shen J, Cooke PS, Robboy SJ, et al. Tissue interactions and estrogenic response during human female fetal reproductive tract development. Differentiation; research in biological diversity. 2018;101:39-45. doi: 10.1016/j.diff.2018.04.002. PubMed PMID: 29684808; PubMed Central PMCID: PMC5993605.

27. Zaret KS, Carroll JS. Pioneer transcription factors: establishing competence for gene expression. Genes & development. 2011;25(21):2227-41. doi: 10.1101/gad.176826.111. PubMed PMID: 22056668; PubMed Central PMCID: PMC3219227.

28. Slattery M, Zhou T, Yang L, Dantas Machado AC, Gordan R, Rohs R. Absence of a simple code: how transcription factors read the genome. Trends Biochem Sci. 2014;39(9):381-99. doi: 10.1016/j.tibs.2014.07.002. PubMed PMID: 25129887; PubMed Central PMCID: PMC4149858.

29. Wittkopp PJ, Kalay G. Cis-regulatory elements: molecular mechanisms and evolutionary processes underlying divergence. Nat Rev Genet. 2012;13(1):59-69. doi: 10.1038/nrg3095. PubMed PMID: 22143240.

30. Wu H, Nord AS, Akiyama JA, Shoukry M, Afzal V, Rubin EM, et al. Tissue-specific RNA expression marks distant-acting developmental enhancers. PLoS Genet. 2014;10(9):e1004610. doi: 10.1371/journal.pgen.1004610. PubMed PMID: 25188404; PubMed Central PMCID: PMC4154669.

31. Wang Q, Stacy T, Binder M, Marin-Padilla M, Sharpe AH, Speck NA. Disruption of the Cbfa2 gene causes necrosis and hemorrhaging in the central nervous system and blocks definitive hematopoiesis. Proceedings of the National Academy of Sciences of the United States of America. 1996;93(8):3444-9. PubMed PMID: 8622955; PubMed Central PMCID: PMC39628.

523 32. Romano RA, Smalley K, Magraw C, Serna VA, Kurita T, Raghavan S, et al. DeltaNp63
524 knockout mice reveal its indispensable role as a master regulator of epithelial development and
525 differentiation. Development (Cambridge, England). 2012;139(4):772-82. Epub 2012/01/26. doi:
526 10.1242/dev.071191. PubMed PMID: 22274697; PubMed Central PMCID: PMC3265062.
527 33. de Laat W, Duboule D. Topology of mammalian developmental enhancers and their regulatory
528 landscapes. Nature. 2013;502(7472):499-506. doi: 10.1038/nature12753. PubMed PMID: 24153303.
529 34. Cunha GR, Kurita T, Cao M, Shen J, Robboy S, Baskin L. Molecular mechanisms of
530 development of the human fetal female reproductive tract. Differentiation; research in biological
531 diversity. 2017;97:54-72. doi: 10.1016/j.diff.2017.07.003. PubMed PMID: 29053991.
532 35. Smith EK, White MC, Weir HK, Peipins LA, Thompson TD. Higher incidence of clear cell
533 adenocarcinoma of the cervix and vagina among women born between 1947 and 1971 in the United
534 States. Cancer Causes Control. 2012;23(1):207-11. Epub 2011/10/22. doi: 10.1007/s10552-011-
535 9855-z. PubMed PMID: 22015647; PubMed Central PMCID: PMC3230753.
536 36. Goodman A, Zukerberg LR, Nikrui N, Scully RE. Vaginal adenosis and clear cell carcinoma
537 after 5-fluorouracil treatment for condylomas. Cancer. 1991;68(7):1628-32. PubMed PMID: 1893363.
538 37. Dungar CF, Wilkinson EJ. Vaginal columnar cell metaplasia. An acquired adenosis associated
539 with topical 5-fluorouracil therapy. The Journal of reproductive medicine. 1995;40(5):361-6. PubMed
540 PMID: 7608876.
541 38. Bornstein J, Sova Y, Atad J, Lurie M, Abramovici H. Development of vaginal adenosis
542 following combined 5-fluorouracil and carbon dioxide laser treatments for diffuse vaginal
543 condylomatosis. Obstetrics and gynecology. 1993;81(5 (Pt 2)):896-8. PubMed PMID: 8469512.
544 39. McLachlan JA, Newbold RR, Bullock BC. Long-term effects on the female mouse genital tract
545 associated with prenatal exposure to diethylstilbestrol. Cancer Res. 1980;40(11):3988-99. PubMed
546 PMID: 7193511.
547 40. Le Grand F, Grifone R, Mourikis P, Houbron C, Gigaud C, Pujol J, et al. Six1 regulates stem
548 cell repair potential and self-renewal during skeletal muscle regeneration. The Journal of cell biology.

549 2012;198(5):815-32. doi: 10.1083/jcb.201201050. PubMed PMID: 22945933; PubMed Central
550 PMCID: PMC3432771.
551 41. Mills AA, Qi Y, Bradley A. Conditional inactivation of p63 by Cre-mediated excision. Genesis.
552 2002;32(2):138-41. PubMed PMID: 11857801.
553 42. Taniuchi I, Osato M, Egawa T, Sunshine MJ, Bae SC, Komori T, et al. Differential
554 requirements for Runx proteins in CD4 repression and epigenetic silencing during T lymphocyte
555 development. Cell. 2002;111(5):621-33. PubMed PMID: 12464175.
556 43. Yu K, Xu J, Liu Z, Sosic D, Shao J, Olson EN, et al. Conditional inactivation of FGF receptor 2
557 reveals an essential role for FGF signaling in the regulation of osteoblast function and bone growth.
558 Development (Cambridge, England). 2003;130(13):3063-74. Epub 2003/05/21. PubMed PMID:
559 12756187.
560 44. Srinivasan L, Sasaki Y, Calado DP, Zhang B, Paik JH, DePinho RA, et al. PI3 kinase signals
561 BCR-dependent mature B cell survival. Cell. 2009;139(3):573-86. doi: 10.1016/j.cell.2009.08.041.
562 PubMed PMID: 19879843; PubMed Central PMCID: PMC2787092.
563 45. Yang X, Li C, Herrera PL, Deng CX. Generation of Smad4/Dpc4 conditional knockout mice.
564 Genesis. 2002;32(2):80-1. PubMed PMID: 11857783.
565 46. Singh SP, Wolfe A, Ng Y, DiVall SA, Buggs C, Levine JE, et al. Impaired estrogen feedback
566 and infertility in female mice with pituitary-specific deletion of estrogen receptor alpha (ESR1). Biology
567 of reproduction. 2009;81(3):488-96. doi: 10.1095/biolreprod.108.075259. PubMed PMID: 19439729;
568 PubMed Central PMCID: PMC2731984.
569 47. Liu W, Selever J, Wang D, Lu MF, Moses KA, Schwartz RJ, et al. Bmp4 signaling is required
570 for outflow-tract septation and branchial-arch artery remodeling. Proceedings of the National Academy
571 of Sciences of the United States of America. 2004;101(13):4489-94. doi: 10.1073/pnas.0308466101.
572 PubMed PMID: 15070745; PubMed Central PMCID: PMC384774.
573 48. Ohyama T, Groves AK. Generation of Pax2-Cre mice by modification of a Pax2 bacterial
574 artificial chromosome. Genesis. 2004;38(4):195-9. PubMed PMID: 15083520.

49. Kim SY, Cordeiro MH, Serna VA, Ebbert K, Butler LM, Sinha S, et al. Rescue of platinum-damaged oocytes from programmed cell death through inactivation of the p53 family signaling network. Cell Death Differ. 2013;20(8):987-97. Epub 2013/04/20. doi: 10.1038/cdd.2013.31. PubMed PMID: 23598363; PubMed Central PMCID: PMC3705595.

50. Serna VA, Wu X, Qiang W, Thomas J, Blumenfeld ML, Kurita T. Cellular kinetics of *MED12*-mutant uterine leiomyoma growth and regression in vivo. Endocr Relat Cancer. 2018;25(7):747-59. doi: 10.1530/ERC-18-0184. PubMed PMID: 29700012.

Figure legends

Fig 1. Expression patterns of SIX1 in developing female reproductive tract.

(A) Volcano plot displaying differential expressed genes in mouse PD2 uterus and vagina. Genes significantly enriched in vagina and uterus in microarray analysis [12] are marked in red and green, respectively. (B) Immunoblot analysis of SIX1 and RUNX1 expression in PD2 mouse FRT. The vagina was divided into upper and lower half. (C-E) Immunofluorescence assay for RUNX1, SIX1 (green) and TRP63 (red) in the lower FRT of PD1 (C) and PD2 (D, E) mice. Outer–wall of fornix is marker with dotted line (D). In the vaginal fornix (E), RUNX1 is down-regulated in MDE upon expression of TRP63 (white arrows), whereas TRP63 and SIX1 are co-expressed (yellow arrows). Bar = 100 μm (C and D), = 50 μm (E).

Fig 2. SIX1 is a down-stream transcription factor of BMP4-SMAD pathway.

In all figures, outer-wall of fornix is shown on the right side. (A) SIX1 expression is maintained in the vaginal fornix of ΔNp63 cKO mice (PD14) (n ≥ 4). Bar = 50 μm. (B) SIX1 expression in MDE is SMAD4 dependent. At PD2, SIX1 is totally absent in the MDE of *Smad4* cKO mice, which normally express RUNX1 in MDE. Bar = 100 μm. (C) Deletion of *Bmp4* in mesenchymal cells reduces SIX1 in MDE. (D) Violin plot of SIX1 immunostaining signals in the lower MDE of *Bmp4* ms-cHET and ms-

601 cKO mice (n = 3 each). The signal distributions of two groups are significantly different (p<0.01). Bar
602 = 100 μm.
603
604 Fig 3. RUNX1 and FGFR2 modulate expression levels of SIX1 in MDE.
605 (A) Expression of RUNX1 and SIX1 in the lower FTR of PD2 *Runx1* cHET and cKO mice. RUNX1 null
606 vaginal/cervical epithelium is outlined by doted lines. Nuclear expression of SIX1 expression is
607 reduced in the fornices of *Runx1* cKO mice. (B) SIX1 expression patterns in the vaginal fornices of
608 *Runx1* cHET and cKO mice at PD2 and PD4. In the fornix of *Runx1* cKO mice, nuclear expression of
609 SIX1 increases from PD2 to PD4, but the overall expression level of SIX1 in MDE remains low and
610 uneven. (C) Violin plot of SIX1 IF signal distribution in the fornix of PD2 *Runx1* cHET and cKO mice (n
611 ≥ 4 per group). The signal distributions of two groups are significantly different (p<0.01). (D)
612 Expression of SIX1 in the vaginal fornix of *Fgfr2* mutant mice. SIX1 is reduced in the fornix of *Fgfr2*
613 cKO mice, but the SIX1 expression level is restored by expression of MAP2K1^{DD}. (E) Violin plot of
614 SIX1 IF signal distribution in the fornix of PD2 *Fgfr2* cHET, *Fgfr2* cKO and *Fgfr2* cKO with MAP2K1^{DD}
615 (cKO+MK) mice (n = 4 per group). The signal distributions are significantly different among 3 groups
616 (p<0.01). (F) Regulation of SIX1 in cultured uterine explants. 20 ng/ml BMP4 has a weak effect on the
617 expression of SIX1 in UtE. The combination of BMP4 (B), ActA (A) and FGF10 (F) (20 ng/ml each)
618 induced nuclear expression of SIX1 and ΔNp63 in restricted regions of UtE. Replacement of FGF10
619 with *Map2k1*^{DD} transgene (MK) efficiently induced SIX1 and ΔNp63 in UtE. (G) Violin plot of SIX1 IF
620 signal distribution in the UtE of cultured uterine explants (n ≥ 4 per group). The signal distributions are
621 significantly different among groups (p<0.01). Bars = 100 μm.
622
623 Fig 4. SIX1 and RUNX1 collaborate in the activation of ΔNp63 locus in MDE.
624 (A) Six1 cKO mice showed minor defects in ΔNp63 expression in the outer-wall (ow) of vaginal fornix.
625 The ΔNp63 negative epithelial regions are indicated by arrows. (B-D) Gene-does effect of *Six1* and
626 *Runx1* on vaginal cell fate commitment of MDE in the vaginal fornix. The outer fornix wall is on the

627 right side. (B) Expression of ΔNp63 (red) and RUNX1 (green). (C) Proportion of MDE lined with
628 ΔNp63-psotive basal layer on the outer-wall of vaginal fornix. (D) Expression of uterine epithelial
629 marker (PGR, green). The epithelium is highlighted with cytokeratin (red). Bars = 100 μm.
630
631 Fig 5. Dose-dependent function of *Six1*, *Runx1* and *Smad4* in the activation of ΔNp63 locus.
632 (A) Monoallelic loss of *Smad4* exaggerates effects of *Six1* and *Runx1* null alleles on ΔNp63
633 expression (green) in MDE. The outer fornix wall is shown on the right side. Breaks in the ΔNp63-
634 positive basal layer in the inner fornix wall are marked by arrowheads. Bar = 50 μm. (B and C) Basal
635 cell density (TRP63-positive nuclear area per epithelial basement membrane length) in the outer and
636 inner fornix walls of *Six1*, *Runx1* and *Smad4* compound mutant mice. The sample number in each
637 group is marker on the bars. The result is demonstrated by average means ± SD. The comparisons
638 that become significantly different by monoallelic *Smad4* loss are marked with lines, and the groups
639 with significantly higher value are marked with asterisks. * $p< 0.05$, ** $p< 0.01$.
640
641 Fig 6. DES inhibits expression of SIX1 and RUNX1 in the vaginal fornix.
642 (A-C) IF analysis for DES-effects on essential factors in the activation of ΔNp63 locus in MDE. mes;
643 mesenchyme. FRTs are collected from PD2 female mice with/without DES treatment (24 hours after
644 DES-pellet injection). (A) IF assay of SIX1 and RUNX1. (B) Violin plot presentation of SIX1 IF signals
645 in the outer and inner fornix walls of control and DES-treated PD2 mice (n=4 each). SIX1 IF signals in
646 MDE were significantly higher (*** $p< 0.01$) in control than DES-treated mice in both outer and inner
647 fornix walls. (C) IF assay of pSMAD1/5/9 and pMAPK1/3.
648
649 Fig 7. Epithelial ESR1 mediates DES effects on ΔNp63 in developing vagina.
650 (A) Expression patterns of ESR1, RUNX1 and SIX1 in *Esr1* cKO mice (PD3) are indistinguishable
651 from wild type mice. (B and C) Effect of DES on the FRT of *Esr1* cHET and cKO mice (PD3): (B) IF
652 assay of ESR1 (green) and TRP63 (red), (C) IF assay of RUNX1 and pMAPK1/3. (D) Effect of DES

653 on the expression of SIX1 (green) and TRP63 (red) in the fornix of *Map2k1*^{DD} conditional transgenic
654 mice (PD3). The outer-wall (ow) of fornix is marked with dotted lines. Bars = 100 μm.
655
656
657 Fig 8. Model of vaginal epithelial cell fate commitment in MDE. Signals of vaginal mesenchymal
658 factors are transduced to down-stream transcription factors, and the transcription factors dose-
659 dependently activate enhancers of ΔNp63 in MDE. Upon differentiation of VgE, ΔNp63 itself maintains
660 the transcriptional activity of ΔNp63 locus in VgE fate in dependent of vaginal mesenchymal factors.
661 DES-ESR1 activity within MDE causes vaginal adenosis by blocking the vaginal cell fate commitment
662 of MDE interfering the signal transduction. Meanwhile, DES-ESR1 activity in vaginal mesenchymal
663 cells promote activation of ΔNp63 locus in MDE through paracrine mechanisms.
664

665 **Supporting information captions**

666 S1 Fig. (A-C) ECR browser view of *Homo sapiens TRP63*. (D) Contrav 3 analysis. Conserved
667 SMADs:RUNX1 binding sites in the coding region in ΔNp63 exon 1. A boxed region with a colored line
668 in each panel is enlarged in the next panel. (E) The sequence is deleted in the ΔNp63-Cre KI mouse
669 genome.

670

671 S2 Fig. Structure of ΔNp63-iCre-IRES-EGFP transgene. (A) Contra V3 analysis of the putative 5'
672 proximal enhancer (based sequence: mm10 chr16:25801055-25802045). (B) Vector maps of the
673 ΔNp63-iCre-IRES-EGFP transgene (linearized and circular form). (C) Distribution of cells expressed
674 ΔNp63-Cre in the lower FRT of PD21 mice. mEGFP reporter (brown) is detected by IHC.

675

676 S3 Fig. Model: Effect of DES exposure on the signaling pathways in developing vagina.

677

Figure 1

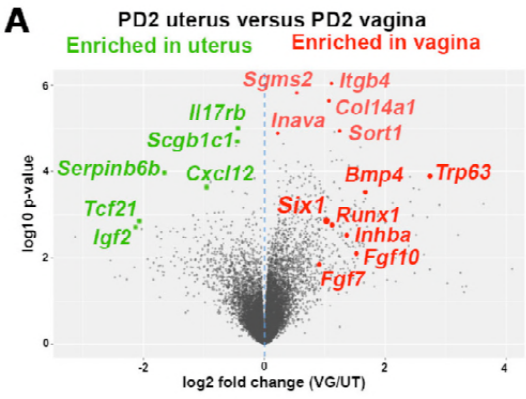
A
PD2 uterus versus PD2 vagina
Enriched in uterus
Enriched in vagina
Sgms2
Itgb4
Il17rb
Col14a1
Inava
Scgb1c1
Sort1
Serpinb6b
Cxcl12
Bmp4
Trp63
Tcf21
Six1
Runx1
Igf2
Inhba
Fgf10
Fgf7
log10 p-value
log2 fold change (VG/UT)

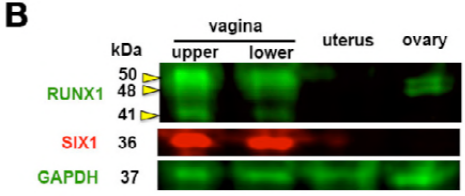
B
vagina
kDa
upper
lower
uterus
ovary
RUNX1
50
48
41
SIX1
36
GAPDH
37

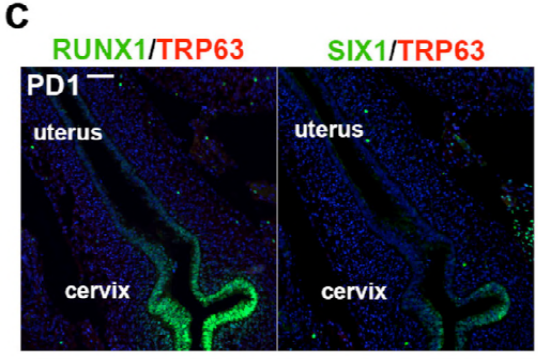
C
RUNX1/TRP63
SIX1/TRP63
PD1
uterus
uterus
cervix
cervix

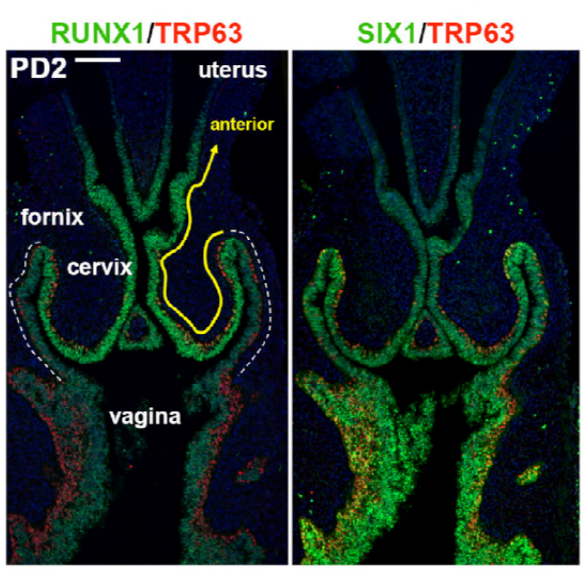
D
RUNX1/TRP63
SIX1/TRP63
PD2
uterus
anterior
fornix
cervix
vagina

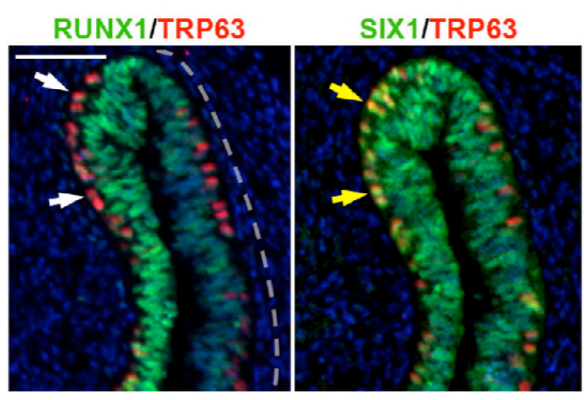
E
RUNX1/TRP63
SIX1/TRP63

Figure 2

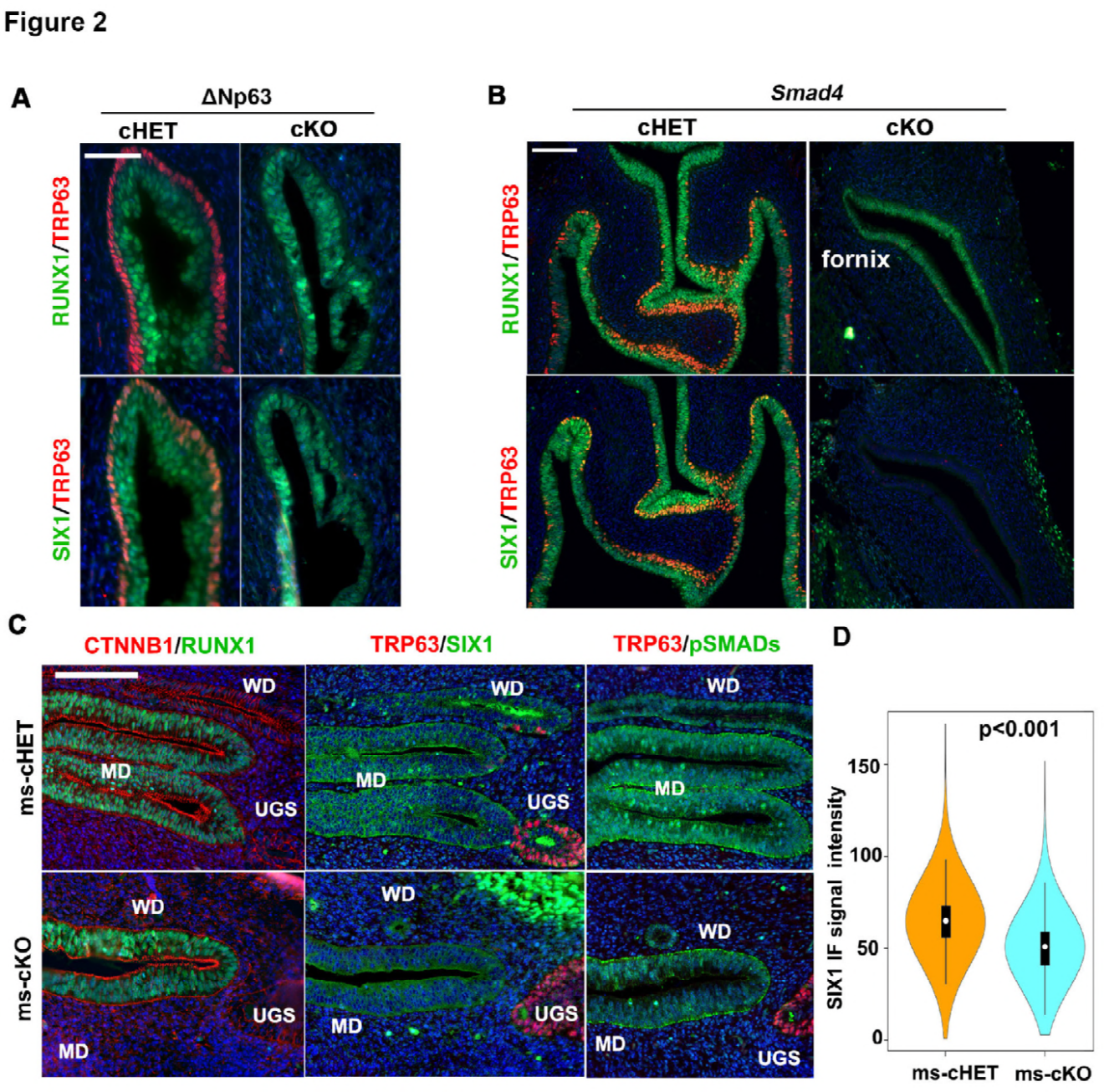
A
ΔNp63
cHET
cKO
RUNX1/TRP63
SIX1/TRP63
B
Smad4
cHET
cKO
RUNX1/TRP63
SIX1/TRP63
fornix
C
CTNNB1/RUNX1
TRP63/SIX1
TRP63/pSMADs
ms-cHET
ms-cKO
WD
MD
UGS
D
p<0.001
SIX1 IF signal intensity
150
100
50
0
ms-cHET
ms-cKO

Figure 3

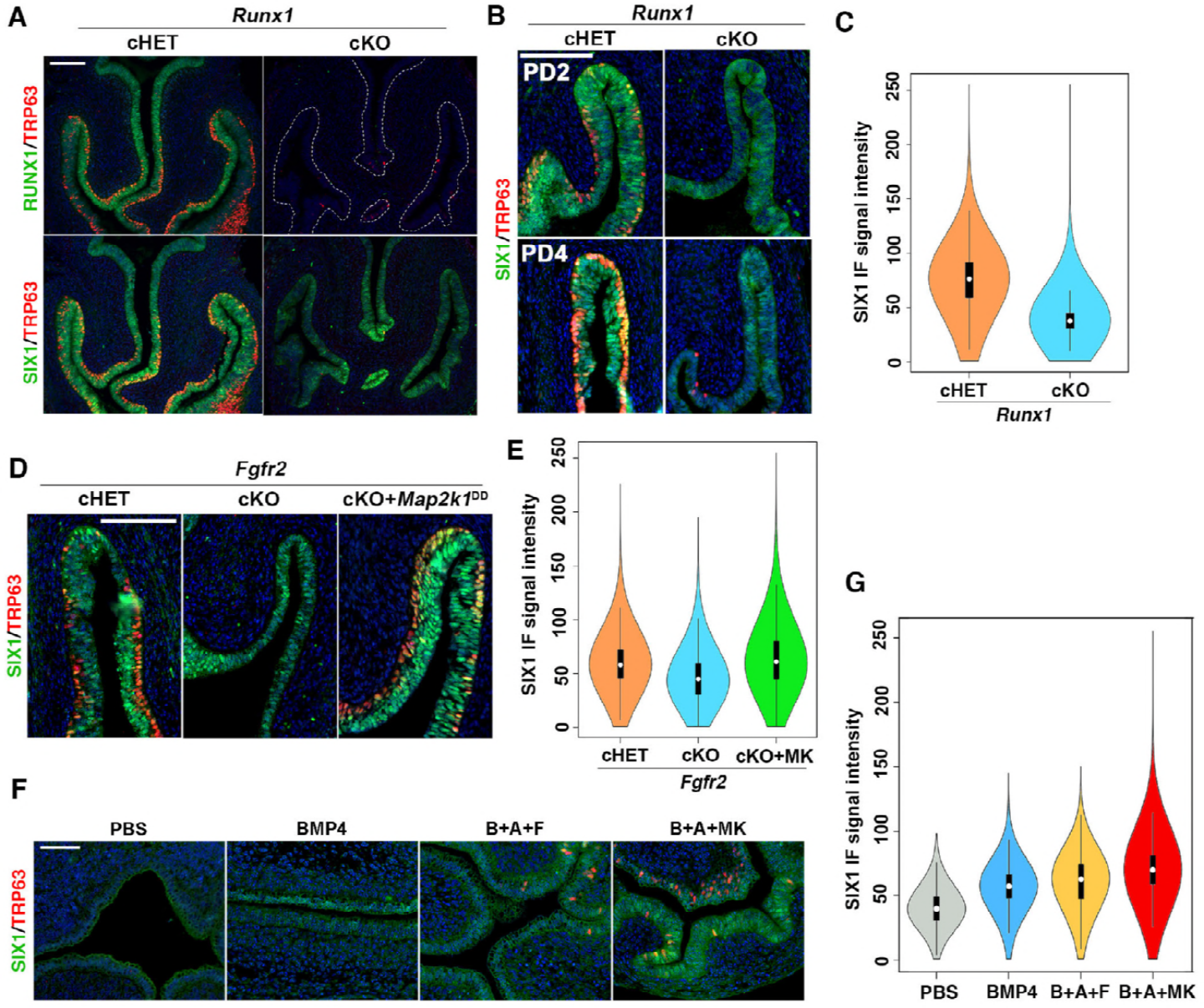
A
Runx1
cHET
cKO
RUNX1/TRP63
SIX1/TRP63
B
Runx1
cHET
cKO
PD2
PD4
SIX1/TRP63
C
SIX1 IF signal intensity
0
50
100
150
200
250
cHET
cKO
Runx1
D
Fgfr2
cHET
cKO
cKO+Map2k1DD
SIX1/TRP63
E
SIX1 IF signal intensity
0
50
100
150
200
250
cHET
cKO
cKO+MK
Fgfr2
F
PBS
BMP4
B+A+F
B+A+MK
SIX1/TRP63
G
SIX1 IF signal intensity
0
50
100
150
200
250
PBS
BMP4
B+A+F
B+A+MK

Figure 4

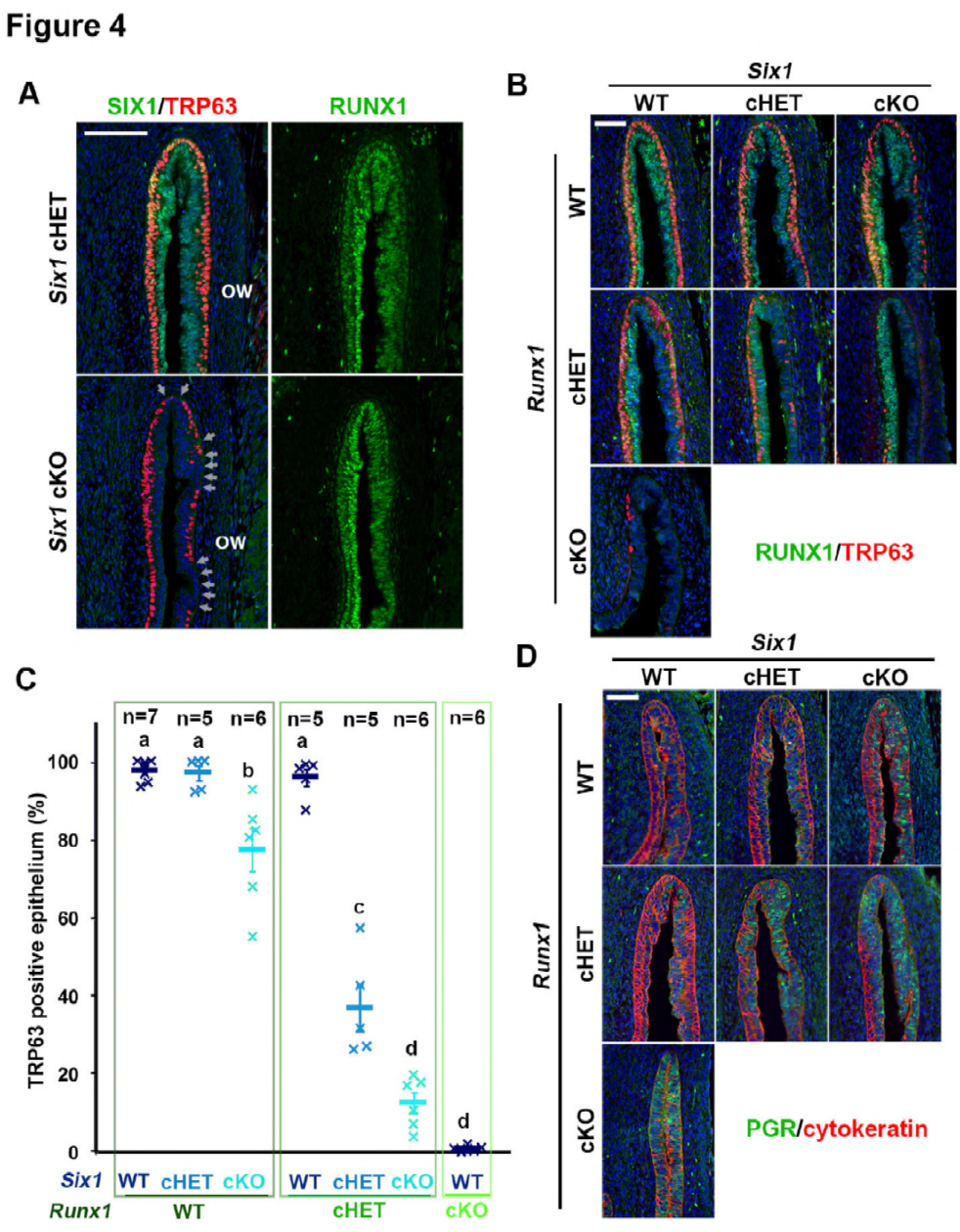
A
SIX1/TRP63
RUNX1
Six1 cHET
Six1 cKO
OW
OW
B
Six1
WT
cHET
cKO
Runx1
WT
cHET
cKO
RUNX1/TRP63
C
TRP63 positive epithelium (%)
n=7
n=5
n=6
n=5
n=5
n=6
n=6
a
a
b
a
c
d
d
Six1
WT
cHET
cKO
WT
cHET
cKO
WT
Runx1
WT
cHET
cKO
D
Six1
WT
cHET
cKO
Runx1
WT
cHET
cKO
PGR/cytokeratin

Figure 5

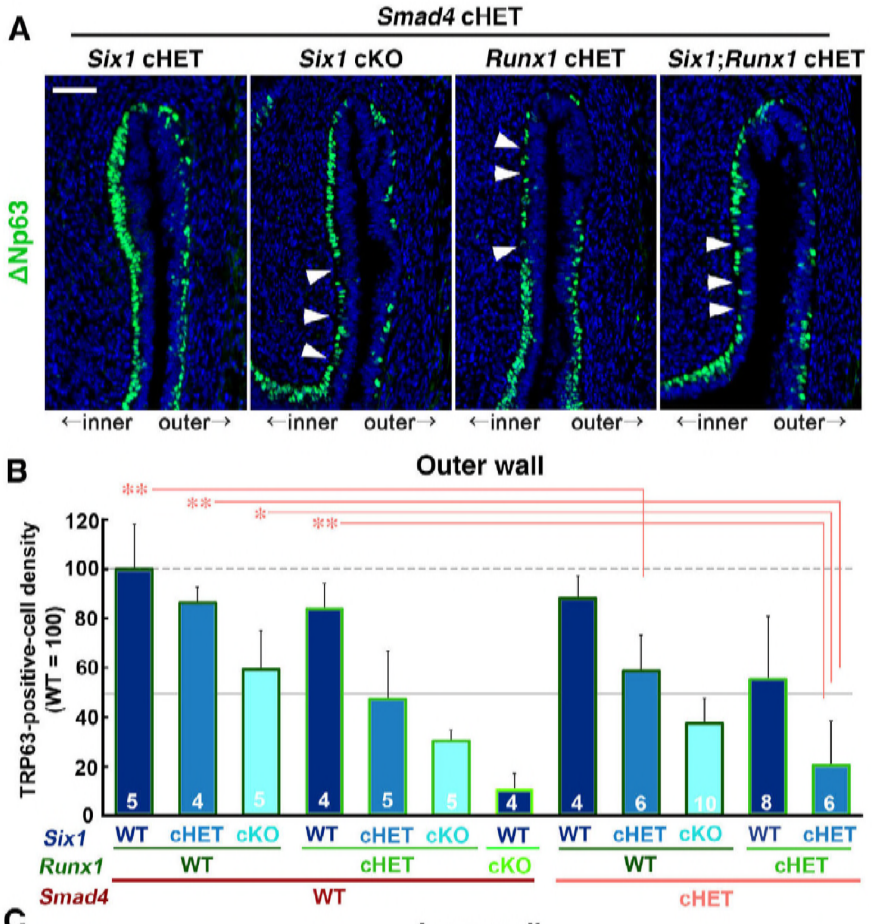
A
Smad4 cHET
Six1 cHET
Six1 cKO
Runx1 cHET
Six1;Runx1 cHET
ΔNp63
←inner outer→
←inner outer→
←inner outer→
←inner outer→
B
Outer wall
TRP63-positive-cell density (WT = 100)
120
100
80
60
40
20
0
**
**
*
**
5
4
5
4
5
5
4
4
6
10
8
6
Six1 WT cHET cKO WT cHET cKO WT WT cHET cKO WT cHET
Runx1 WT cHET cKO WT cHET
Smad4 WT cHET
C
Inner wall
TRP63-positive-cell density (WT = 100)
120
100
80
60
40
20
0
***
**
*
**
*
5
4
5
4
5
5
4
4
6
10
8
6
Six1 WT cHET cKO WT cHET cKO WT WT cHET cKO WT cHET
Runx1 WT cHET cKO WT cHET
Smad4 WT cHET

Figure 6

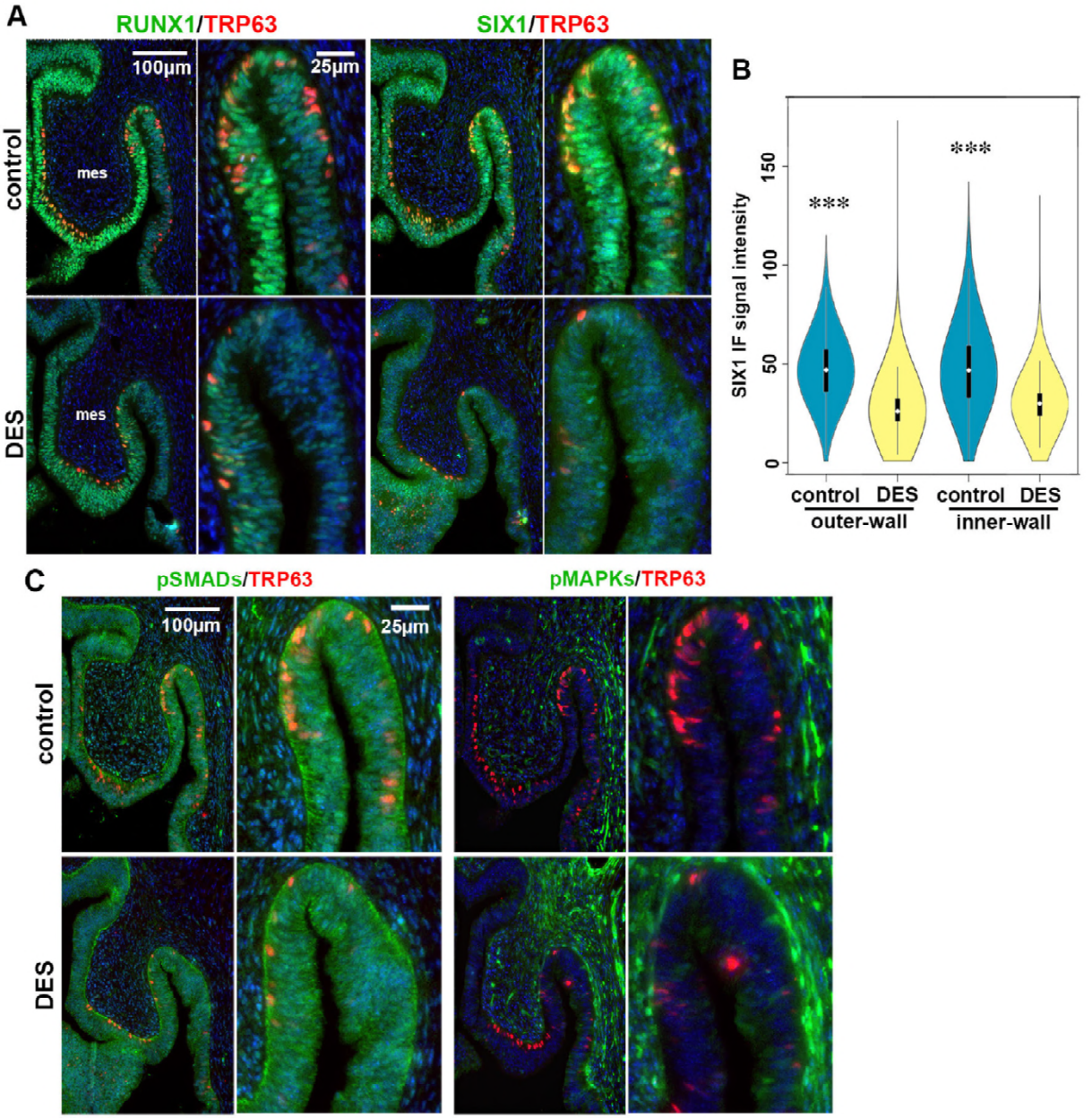
A
RUNX1/TRP63
SIX1/TRP63
100μm
25μm
control
DES
mes
mes
B
SIX1 IF signal intensity
0
50
100
150
***
***
control
DES
control
DES
outer-wall
inner-wall
C
pSMADs/TRP63
pMAPKs/TRP63
100μm
25μm
control
DES

Figure 7

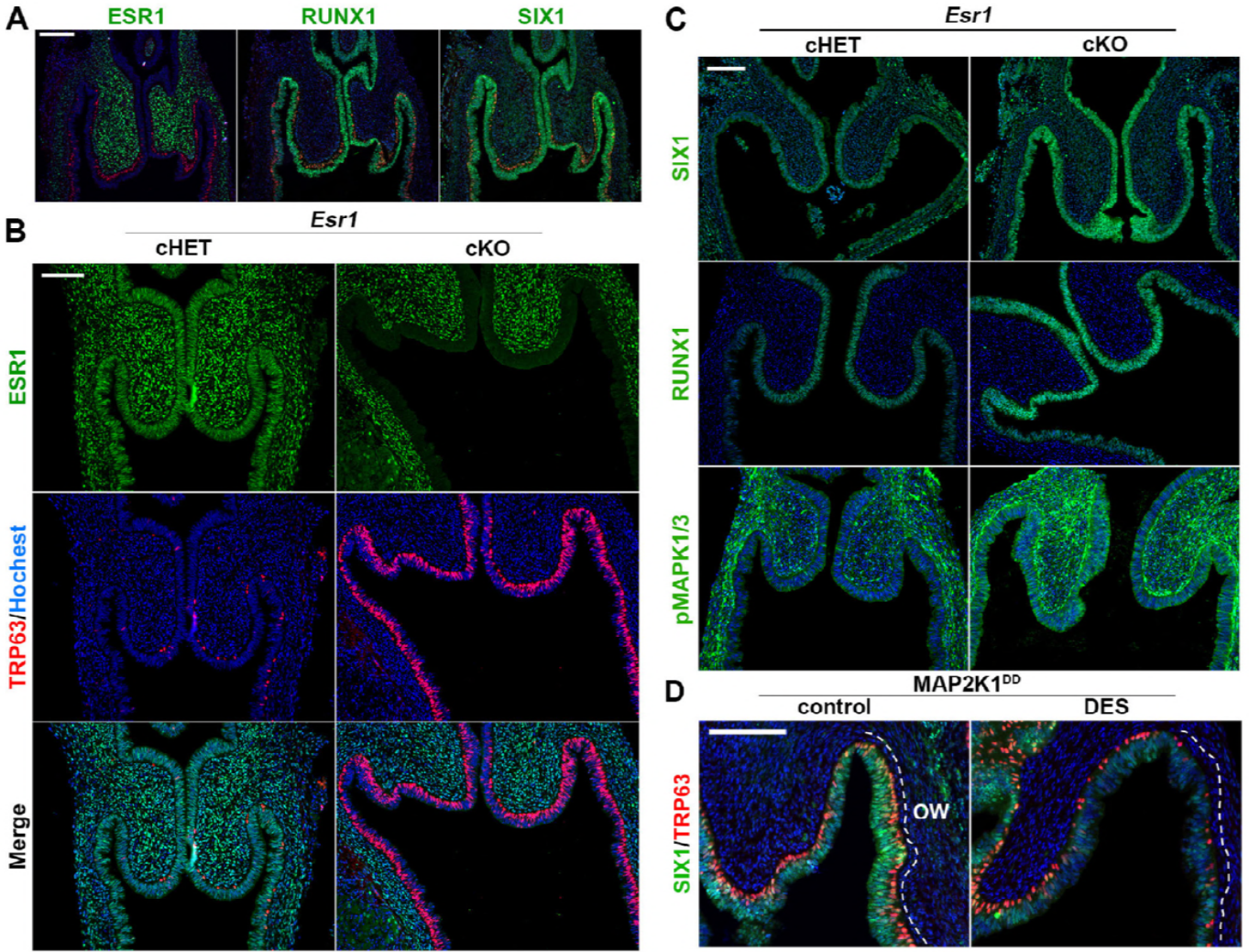
A
ESR1
RUNX1
SIX1
B
Esr1
cHET
cKO
ESR1
TRP63/Hochest
Merge
C
Esr1
cHET
cKO
SIX1
RUNX1
pMAPK1/3
D
MAP2K1DD
control
DES
SIX1/TRP63
OW

Figure 8

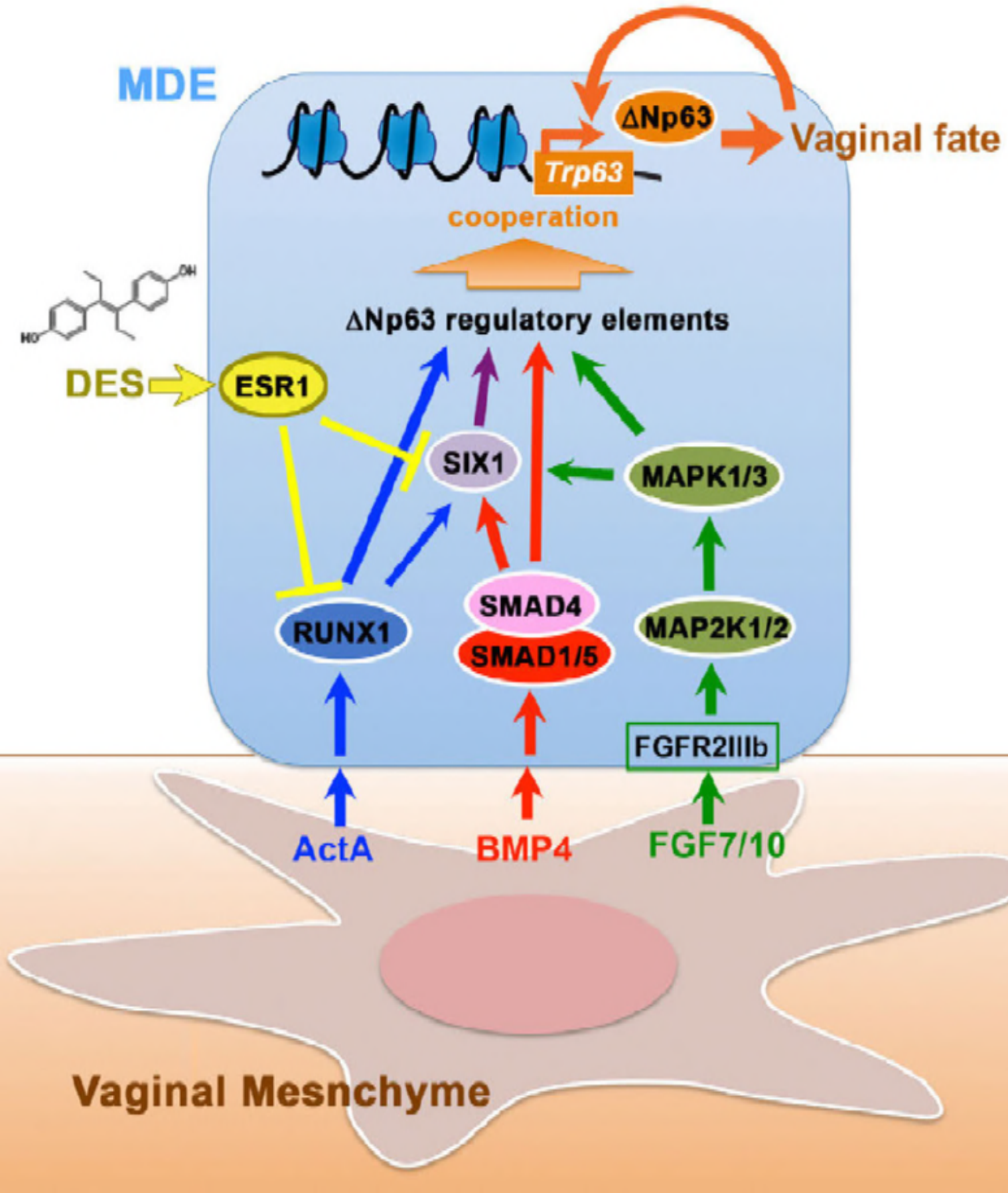
MDE
ΔNp63
Vaginal fate
Trp63
cooperation
ΔNp63 regulatory elements
DES
ESR1
SIX1
MAPK1/3
RUNX1
SMAD4
SMAD1/5
MAP2K1/2
FGFR2IIIb
ActA
BMP4
FGF7/10
Vaginal Mesnchyme

S1 Figure

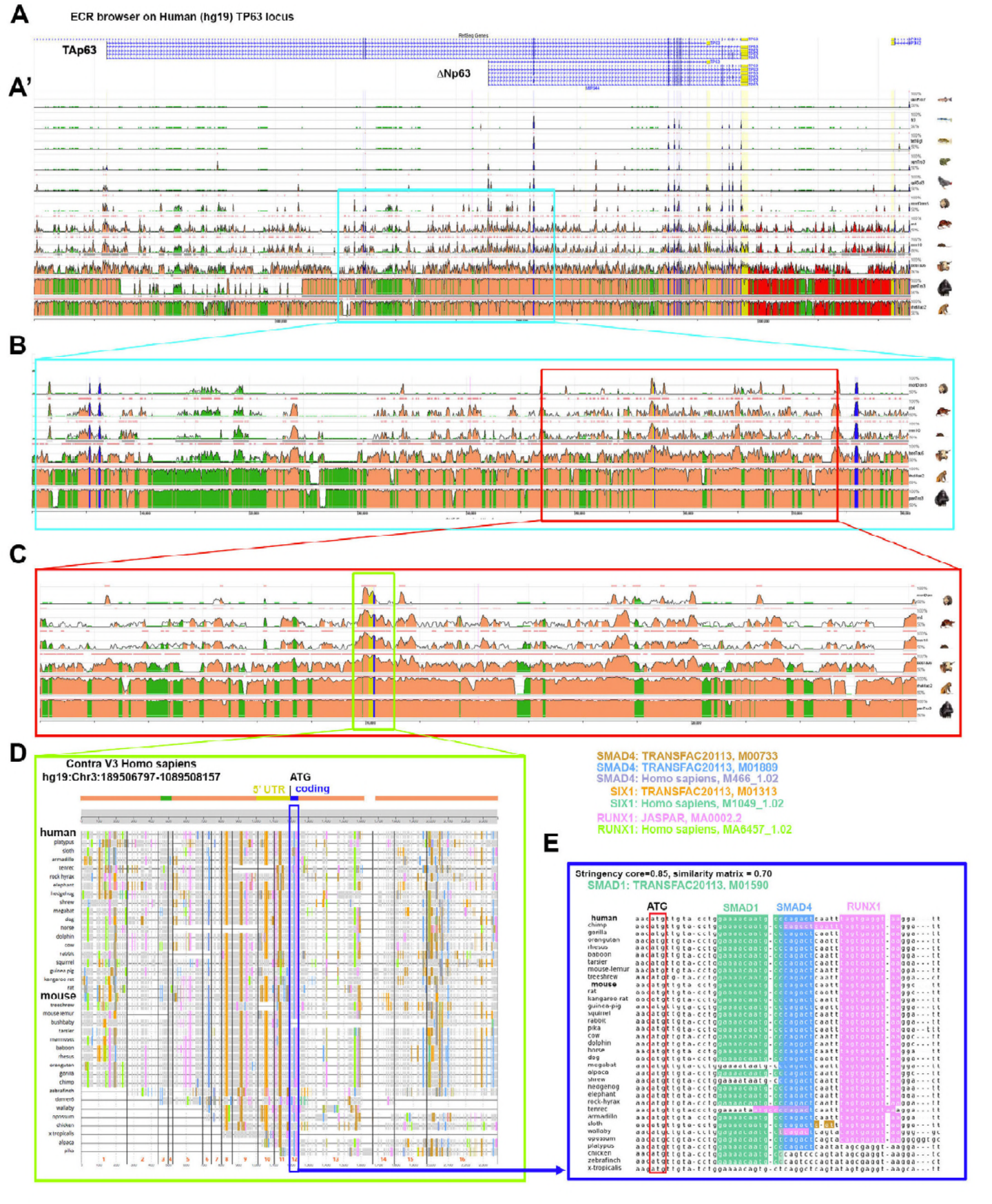
A
ECR browser on Human (hg19) TP63 locus
TAp63
ΔNp63
A'
B
C
D
Contra V3 Homo sapiens
hg19:Chr3:189506797-1089508157
ATG
5' UTR
coding
human
mouse
SMAD4: TRANSFAC20113, M00733
SMAD4: TRANSFAC20113, M01089
SMAD4: Homo sapiens, M466_1.02
SIX1: TRANSFAC20113, M01313
SIX1: Homo sapiens, M1049_1.02
RUNX1: JASPAR, MA0002.2
RUNX1: Homo sapiens, MA6457_1.02
E
Stringency core=0.85, similarity matrix = 0.70
SMAD1: TRANSFAC20113, M01590
ATG
SMAD1
SMAD4
RUNX1

S2 Fig

A

mouse (mm10)
rat
orangutan
human (hg18)
chimp
marmoset
rhesus
treeshrew
shrew
dog
horse
cow
elephant
bushbaby
guinea pig
tenrec
Six-1 TRANSFAC20113,M01313
SIX1 Homo_sapiens,M1049_1.02
RUNX1 Homo_sapiens,M6457_1.02
RUNX1 JASPAR_CORE_2016,MA0002.2
SMAD4 Homo_sapiens,M6466_1.02
SMAD4 TRANSFAC20113,SMAD4_Q6,M00733
Smad4 TRANSFAC20113,SMAD4_Q6_01,M01889

B

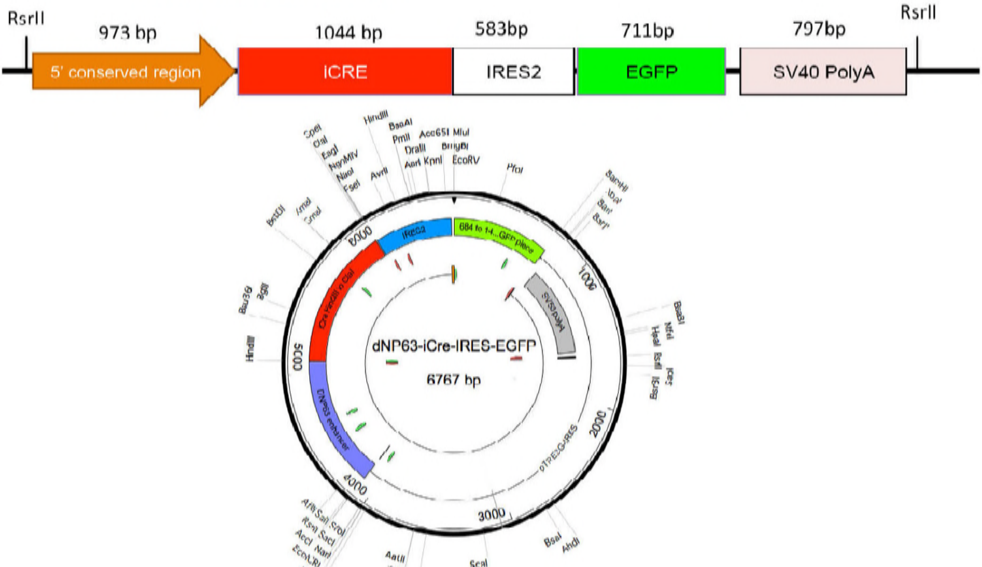

RsrII
973 bp
5' conserved region
1044 bp
iCRE
583bp
IRES2
711bp
EGFP
797bp
SV40 PolyA
RsrII
dNP63-iCre-IRES-EGFP
6767 bp

C

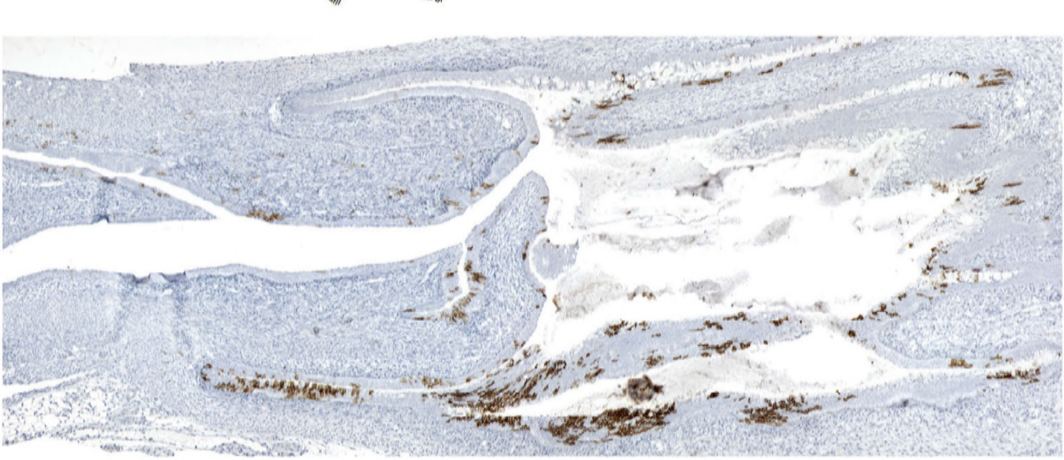

S3 Figure

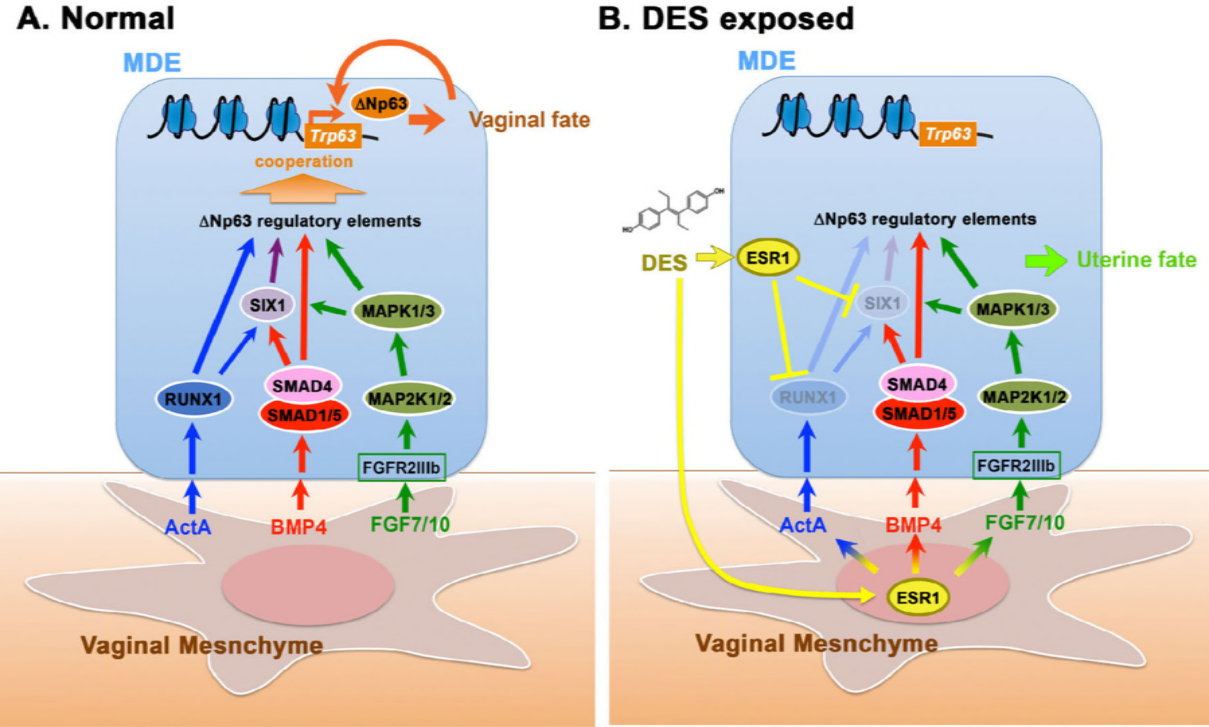
A. Normal
MDE
ΔNp63
Trp63
Vaginal fate
cooperation
ΔNp63 regulatory elements
SIX1
MAPK1/3
RUNX1
SMAD4
SMAD1/5
MAP2K1/2
FGFR2IIIb
ActA
BMP4
FGF7/10
Vaginal Mesnchyme
B. DES exposed
MDE
Trp63
ΔNp63 regulatory elements
DES
ESR1
Uterine fate
SIX1
MAPK1/3
RUNX1
SMAD4
SMAD1/5
MAP2K1/2
FGFR2IIIb
ActA
BMP4
FGF7/10
ESR1
Vaginal Mesnchyme